THE JOURNAL OF BIOLOGICAL CHEMISTRY VOL. 287, NO. 16, pp. 13137–13158, April 13, 2012
Published in the U.S.A.

Molecular Basis for Failure of "Atypical" C1 Domain of Vav1 to Bind Diacylglycerol/Phorbol Ester*[S]

Received for publication, November 2, 2011, and in revised form, February 16, 2012 Published, JBC Papers in Press, February 18, 2012, DOI 10.1074/jbc.M111.320010

Tamas Geczy[‡], Megan L. Peach[§], Saïd El Kazzouli[¶], Dina M. Sigano[¶], Ji-Hye Kang[¶], Christopher J. Valle[‡], Julia Selezneva[‡], Wonhee Woo[‡], Noemi Kedei[‡], Nancy E. Lewin[‡], Susan H. Garfield[‖], Langston Lim[‖], Poonam Mannan[‖], Victor E. Marquez[¶], and Peter M. Blumberg[‡1]

From the [‡]Laboratory of Cancer Biology and Genetics and [‖]Laboratory of Experimental Carcinogenesis, Center for Cancer Research, NCI, National Institutes of Health, Bethesda, Maryland 20892 and the [¶]Chemical Biology Laboratory, Molecular Discovery Program, Center for Cancer Research, and [§]Basic Research Program, SAIC-Frederick, NCI-Frederick, National Institutes of Health, Frederick, Maryland 21702

Background: The C1 domain of Vav1 retains a three-dimensional structure consistent with phorbol ester binding but nevertheless does not bind.
Results: Five residues render the C1 domain less lipophilic and interfere with its binding.
Conclusion: The C1 domain of Vav1 illustrates a novel mechanism rendering the C1 domain "atypical."
Significance: Ligands exploiting the specific amino acid differences may selectively target Vav1.

C1 domains, the recognition motif of the second messenger diacylglycerol and of the phorbol esters, are classified as typical (ligand-responsive) or atypical (not ligand-responsive). The C1 domain of Vav1, a guanine nucleotide exchange factor, plays a critical role in regulation of Vav activity through stabilization of the Dbl homology domain, which is responsible for exchange activity of Vav. Although the C1 domain of Vav1 is classified as atypical, it retains a binding pocket geometry homologous to that of the typical C1 domains of PKCs. This study clarifies the basis for its failure to bind ligands. Substituting Vav1-specific residues into the C1b domain of PKCδ, we identified five crucial residues (Glu[9], Glu[10], Thr[11], Thr[24], and Tyr[26]) along the rim of the binding cleft that weaken binding potency in a cumulative fashion. Reciprocally, replacing these incompatible residues in the Vav1 C1 domain with the corresponding residues from PKCδ C1b (δC1b) conferred high potency for phorbol ester binding. Computer modeling predicts that these unique residues in Vav1 increase the hydrophilicity of the rim of the binding pocket, impairing membrane association and thereby preventing formation of the ternary C1-ligand-membrane binding complex. The initial design of diacylglycerol-lactones to exploit these Vav1 unique residues showed enhanced selectivity for C1 domains incorporating these residues, suggesting a strategy for the development of ligands targeting Vav1.

The lipophilic second messenger *sn*-1,2-diacylglycerol (DAG)[2] plays a central role in cellular signaling. Following the activation of many receptors, DAG is generated either through the hydrolysis of phosphatidylinositol 4,5-bisphosphate via phospholipase C or indirectly from phosphatidylcholine via phospholipase D (1). Its downstream effects are mediated through interaction with protein kinase C (PKC), RasGRP, and five other families of effectors that possess a C1 domain recognition motif (2–4). The profound involvement of PKC and these other families of signaling proteins in proliferation, differentiation, apoptosis, angiogenesis, and drug resistance has emphasized the importance of these C1 domain-containing proteins as therapeutic targets for cancer and other diseases, and multiple agents, *e.g.* bryostatin 1 or PEP005, targeted to the C1 domains of PKC are currently in clinical trials (4, 5).

Structural studies by NMR, x-ray crystallography, and molecular modeling have afforded substantial insights into ligand recognition by the C1 domains (6–9). These domains are cysteine-rich zinc finger structures. The DAG-binding site is a hydrophilic cleft formed from two pulled apart β-sheets, whereas the C1 domain surface surrounding the binding cleft is hydrophobic. Insertion of DAG into the binding cleft serves to complete the hydrophobic surface, and additional hydrophobicity is contributed by hydrophobic substituents on the DAG. This increase in hydrophobicity upon binding promotes insertion of the C1 domain into the lipid bilayer, which in turn can drive conformational change in the overall protein structure, as is the case with PKC, as well as promote translocation to the membrane, changing access of the protein to interacting partners. Because the lipids of the bilayer interact both with the ligand and with the surface of the C1 domain, great selectivity is possible. Although DAG represents the endogenous ligand for the C1 domains, nature has provided a diversity of high affinity analogs such as the phorbol esters or bryostatins, and DAG-lactones have afforded a powerful synthetic platform for probing structure-function relationships (4, 10).

* This work was supported, in whole or in part, by National Institutes of Health Project Z1A BC 005270 from the Intramural Research Program, NCI.
[S] This article contains supplemental Figs. 1–3.
[1] To whom correspondence should be addressed: National Institutes of Health, NCI, Bldg. 37, Rm. 4048, 37 Convent Dr., MSC 4255, Bethesda MD 20892-4255. Tel.: 301-496-3189; Fax: 301-496-8709; E-mail: blumberp@dc37a.nci.nih.gov.
[2] The abbreviations used are: DAG, diacylglycerol; GEF, guanyl exchange factor; DH domain, Dbl homology domain; PH domain, pleckstrin homology domain; PMA, phorbol 12-myristate 13-acetate; PDBu, phorbol 12,13-dibutyrate; MLP, molecular lipophilicity; DOG, 1,2-dioctanoyl glycerol; PS, phosphatidylserine; PC, phosphatidylcholine; SH, Src homology.

Initially, C1 domains were categorized into two families (11) as follows: (i) those that bound DAG/phorbol ester were termed "typical," and (ii) the more divergent members that failed to bind were termed "atypical." Examples of atypical C1 domains include those of the atypical PKC isozymes (aPKCζ and aPKCι), c-Raf, kinase suppressor of Ras (KSR), and Vav (3, 4, 12). More recently, it has become evident that atypical C1 domains can be further categorized. The first subclass, represented by proteins like c-Raf or KSR, consists of C1 domains that are grossly distorted in the binding cleft geometry (*e.g.* deletions of several key residues in the loops making up the binding pocket). Members of the second subclass, in contrast, retain the binding cleft geometry but incorporate other factors impeding ligand binding. We showed that, in the case of the atypical PKCs, a series of three arginine residues lining the rim of the binding pocket were able to rotate into the cleft, making it inaccessible to ligands (13). Replacement of these arginine residues with the corresponding residues found in the C1b domain of PKCδ generated high affinity ligand binding and ligand-driven membrane translocation.

Recent structural studies using x-ray crystallography have revealed a striking resemblance between the binding pocket geometry of the C1b domain of the potent phorbol ester receptor PKCδ and that of the protooncogene Vav1, a guanine nucleotide exchange factor (14–16). Although early studies on the GEF activity of Vav1 toward small GTPases suggested a DAG/phorbol ester-sensitive function of Vav1 (17), subsequent ligand-binding experiments using purified recombinant Vav1 and the ultrapotent phorbol ester analog [^{3}H]bryostatin did not support those results (18), leading to the classification of this C1 domain as atypical. In this study, we have sought to identify key structural determinants in the Vav1 C1 sequence that (analogous to our findings with atypical PKCs) might account for its apparent lack of affinity for DAG and phorbol esters.

Vav1 is a versatile cellular signal transducer molecule that plays a pivotal role in various signaling pathways. One of the most important and best characterized functions of Vav1 is the GEF activity toward the Rho/Rac family of small GTPases, which are important molecular transducers in signaling cascades that regulate cytoskeleton organization, cell cycle progression, gene transcription, adhesion, migration, cell growth, and survival (19–21). In addition to their activity as exchange factors for Rho/Rac proteins, Vav proteins can also regulate various other cellular processes in a GEF-independent fashion, functioning as adapter molecules to facilitate protein-protein interactions (22). The expression of Vav1 is restricted almost exclusively to normal cells of hematopoietic origin (23–25). There, T-cell receptor-coupled activation of the guanine exchange function of Vav1 leads to Rac1-induced cytoskeleton organization, an essential step for the formation of the immunological synapse and subsequent proper T-cell activation (20, 26). Vav1 further plays a crucial role in T-cell development (27). Although less extensively investigated, recent studies have also characterized a role of Vav1 in human cancer, especially in solid tumors of nonhematopoietic origin (28), where the ectopic expression of wild-type Vav1 can contribute to the development and progression of these malignancies (29–32). It therefore represents an attractive therapeutic target, both for cancer as well as for autoimmunity.

Vav1 possesses multiple structural motifs that mediate its versatile functions in cellular signaling (Fig. 1*A*) (19). It contains a Dbl homology (DH) domain, which is responsible for catalyzing nucleotide exchange (33). The DH domain is flanked by an N-terminal acidic (Ac) motif and a calponin homology (CH) domain together with a C-terminal pleckstrin homology (PH) domain and a C1 domain. These domains surrounding the catalytic DH domain in the CH-C1 segment of the molecule regulate the exchange activity of Vav1 (28). In addition, the structure of Vav contains an SH3-SH2-SH3 cassette at the C terminus, which links it with tyrosine phosphorylation pathways and mediates its activity as a scaffold protein (22).

Initial studies of Vav using site-directed mutagenesis identified the C1 domain as critical for maintaining efficient guanine nucleotide exchange activity toward Rho/Rac GTPases (34, 35). Although this regulatory effect initially was hypothesized to arise from direct contacts between the C1 domain and the GTPases (36), crystallographic studies now provide a different explanation (15, 16). An intramolecular network of contacts between the PH-C1 unit and the DH domain helps stabilize the conformation of a critical α-helix within the DH domain, which is essential for the displacement of guanine nucleotide from the GTPase. The C1 domain (together with the PH domain) thus contributes to optimal GEF activity by restricting the conformational flexibility of the DH domain, keeping it in a stable conformation primed for efficient interaction with the Rac1 GTPase. The C1 domain of Vav1 possesses a three-dimensional structure very similar to that of the typical C1b domain of PKCδ. Because its solvent-accessible cavity is located in the vicinity of the α-helix of DH that makes contacts with Rac1, ligand binding to the cleft has the intriguing potential to modulate Vav1 function. Could DAG/phorbol esters or their derivatives interact with this binding pocket and thereby disrupt the enzymatic function of Vav1?

In this study we wished to characterize the ligand binding properties of the C1 domain of Vav1. We confirmed the lack of phorbol ester binding of Vav1. Using site-directed mutagenesis, we identified the central structural determinants in the loops making up the binding cleft responsible for the lack of phorbol ester sensitivity. The C1 domain of Vav1 (together with that of atypical PKCs) thus belongs to that subclass of atypical (nonresponsive) C1 domains that retain the proper structure for ligand binding. However, the presence of four unique hydrophilic residues around the rim of the binding pocket disrupts the lipophilic surface of the tip of the binding pocket and, together with an inappropriately hydrophobic residue distal to the tip of the C1 domain, interferes with the insertion of ligand receptor complex into the lipid membrane, which is an essential step for stabilizing the ternary binding complex of ligand receptor and membrane. Mutating these residues in the Vav1 C1 domain to correspond to the ones in the potent phorbol ester receptor δC1b, we demonstrated almost complete recovery of binding affinity *in vitro* and *in vivo*, which confirms the previous structural findings on the conserved binding pocket geometry of Vav1. Our results raise the possibility that appropriately modified DAG/phorbol ester analogs that can specifi-

cally target these residues might have the potential to selectively bind to Vav1 C1 and to manipulate Vav1 function through this interaction. Finally, we describe some DAG-lactones that display modest selectivity for features of the Vav1-C1-like structure.

EXPERIMENTAL PROCEDURES

Materials—[20-^{3}H]Phorbol 12,13-dibutyrate ([^{3}H]PDBu) (17.2 Ci/mmol) was obtained from PerkinElmer Life Sciences. PDBu and phorbol 12-myristate 13-acetate (PMA) were purchased from LC Laboratories (Woburn, MA). Phosphatidyl-L-serine (PS), phosphatidylcholine (PC), and 1,2-dioctanoylglycerol (DOG) were from Avanti Polar Lipids (Alabaster, AL). LNCaP human prostate cancer cells, fetal bovine serum (FBS), RPMI 1640 medium, and L-glutamine were from the American Type Culture Collection (Manassas, VA). Reagents used for culturing bacteria (LB Broth, LB agar plates with different selection antibiotics, etc.) were from K-D Medical, Inc. (Columbia, MD). The oligonucleotide primers used for PCR cloning, sequence analysis, and site-directed mutagenesis were obtained from Invitrogen.

Construction of GST-fused C1 Domains of PKCδ and Vav1—The wild-type δC1b domain in a pGEX-5×-1 plasmid (GE Healthcare) had previously been constructed in our laboratory (48). To generate a recombinant Vav1 C1 domain fused to glutathione *S*-transferase (GST) at the N terminus, PCR amplification of the appropriate sequence was performed using Platinum® PCR SuperMix High Fidelity (Invitrogen), according to the manufacturer's instructions. The full-length cDNA clone of Vav1 served as template. The following oligonucleotide primers were used in the PCR as follows: (i) forward primer 5′-CGGAATTCAATGCTACAGCCAATGGGC-3′ and (ii) reverse primer 5′-CGGAATTCGAAATCTTGCCCATGGCG-3′. The DNA fragments of the PCR were purified with QIAquick PCR purification kit (Qiagen, Inc., Valencia, CA) and subsequently digested with EcoRI (New England Biolabs, Beverly, MA) to create adhesive ends of the C1 fragments. After an additional step of purification with the QIAquick PCR purification kit, the fragments were finally ligated into the GST-containing pGEX-5×-1 plasmid (GE Healthcare) using the EcoRI restriction sites. Analysis of the DNA sequence of the construct was conducted by the DNA Minicore (Center for Cancer Research, NCI, National Institutes of Health). Verification of the sequencing data was performed using the following software: BioEdit Sequence Alignment Editor Version 7.0.5 and DNA Baser Sequence Assembler Version 2.91.

Site-directed Mutagenesis of the C1b Domain of PKCδ and the C1 Domain of Vav1—C1 domains consisted of a conserved 50–51-amino acid sequence possessing the characteristic cysteine-rich motif $HX_{12}CX_2CX_nCX_2CX_4HX_2CX_7C$, where H is histidine, C is cysteine, *X* is any other amino acid, and *n* is 13 or 14 (Fig. 2, *gray-shaded letters*) (11). To facilitate comparisons between C1 domains, we will refer to residues using numbering internal to the C1 domain itself, with the N-terminal histidine residue being labeled His^1. This residue corresponds to His^{516} in full-length Vav1 and His^{231} in the C1b domain of full-length PKCδ. Point mutations of the amino acid residues at positions 9, 10, 11, 22, 24, and 26 of both PKCδ C1b and Vav1 C1 were introduced using the GeneTailor™ site-directed mutagenesis system (Invitrogen) according to the manufacturer's instructions. To generate the C1 domain mutants of PKCδ and Vav1, the above mentioned wild-type C1 constructs (PKCδ and Vav1) in pGEX-5×-1 were used. Single, double, and triple mutations were introduced in one step, and quadruple and quintuple mutants were generated in a stepwise fashion using triple mutants as templates. The presence of mutations was verified by DNA sequencing (DNA Minicore) and analysis (BioEdit, DNA Baser).

Construction of GFP-labeled C1 Domains of PKCδ and Vav1—To generate GFP-tagged fluorescent fusion proteins for *in vivo* translocation studies, pGEX-5×-1 plasmids containing recombinant C1 domain sequences from either PKCδ or Vav1 were digested with EcoRI (New England Biolabs). The DNA fragments from this reaction were purified with the QIAquick PCR purification kit (Qiagen). Finally, the C1 fragments were ligated into the pEGFP-C2 vector (Clontech) using the EcoRI restriction sites, and the DNA sequences of the constructs were confirmed by sequence analysis (DNA Minicore).

Construction of Full-length Vav1 (Wild-type, Triple, and Quintuple Mutant) Fused to GFP—The GFP-tagged wild-type Vav1 was generated using the pENTR™ Directional TOPO® cloning kit (Invitrogen), according to the instructions described in the manual. Briefly, PCR amplification of the appropriate full-length Vav1 sequence was first carried out using Platinum® PCR SuperMix High Fidelity (Invitrogen). The cDNA clone of Vav1 served as a template, and the following oligonucleotide primers were applied in the PCR: (i) forward primer 5′-CACCGAGCTCTGGCGACAGTGC-3′ and (ii) reverse primer 5′-TCAGCAATATTCGGAATAGTCTTCC-3′. The PCR product was then TOPO-cloned into a pENTR™/D-TOPO® vector, which served as an Entry clone. Next, using the LR recombination reaction of the Gateway method (Invitrogen), we transferred the appropriate full-length Vav1 sequence from the Entry vector into a pcDNA-DEST53 Gateway™ destination vector (Invitrogen), which encodes an N-terminal GFP tag. The triple (E9M/E10S/T11P) and the quintuple (E9M/E10S/T11P/T24L/Y26K) mutants of the full-length Vav1 were generated using the GeneTailor™ site-directed mutagenesis system (Invitrogen) described above for the C1 domain mutants. The TOPO-Entry clone of the (full length) wild-type Vav1 served as a template for constructing the triple and quintuple mutants in a stepwise fashion. The mutated Entry clones were then subcloned into pcDNA-DEST53 using the above mentioned LR recombination reaction. The DNA sequences of the GFP-tagged full-length constructs were verified by sequence analysis (DNA Minicore).

Expression and Purification of GST-tagged C1 Domains from Escherichia coli—The C1 domains of both PKCδ and Vav1 in the pGEX-5×-1 plasmid were transformed into BL21-AI™ One Shot® chemically competent *E. coli* (Invitrogen). Transformants were grown in LB broth medium (K-D Medical) at 37 °C until the optical density of the bacterial suspension reached 0.6–0.8. Expression of the GST fusion proteins was induced with 0.3 mM isopropyl *O*-D-thiogalactopyranoside and 0.125% L-arabinose (both from Sigma) for 4 h at 37 °C. Bacterial cells were subjected to sonication in B-PER® bacterial protein

extraction reagent, supplemented with 50 mg/ml lysozyme and 2500 units/ml DNase I (all from Pierce). The expressed GST-tagged C1 proteins were purified using a B-PER GST spin purification kit (Pierce) according to the manufacturer's instructions. Purification efficiency was evaluated by SDS-PAGE analysis. Protein concentration was assessed with the protein assay kit from Bio-Rad. Purified fusion proteins were stored in 30% glycerol at −80 °C.

In Vitro ([^{3}H]PDBu Assays—To assess the affinity of the different C1 domains (wild-type and mutant PKCδ and Vav1) to phorbol esters, purified proteins were subjected to an *in vitro* [^{3}H]PDBu binding assay, and the dissociation constants (K_d values) of the individual C1 domains were determined. Measurement of [^{3}H]PDBu binding, using the polyethylene glycol precipitation assay developed in our laboratory, was described in detail previously (37). Competitive binding assays were carried out to assess the affinities (K_i values) of DOG and DAG-lactones as described in detail elsewhere (38). Triton X-100, included in some of the assays, did not exceed 0.003%.

Translocation of GFP-labeled Proteins—LNCaP cells (between passage numbers 5 and 20) were plated at a density of 60,000 cells/plate on Ibidi dishes (Ibidi, LLC, Verona, WI) and subcultured at 37 °C in RPMI 1640 medium supplemented with 10% FBS and 2 mM L-glutamine. After 48 h in culture, cells were transfected with GFP-tagged recombinant constructs, using Lipofectamine reagent and Plus reagent (both from Invitrogen) according to the manufacturer's protocol. Cellular expression of fluorescent fusion proteins was examined 24 h after transfection on a Zeiss LSM 510 NLO confocal microscopy system (Carl Zeiss, Inc., Thornwood, NY) with excitation from a 30-milliwatt argon laser tuned to 488 nm and emission collected with a BP 500–530 filter. Intracellular translocation of the GFP-labeled C1 domains upon PMA treatment was detected sequentially after the administration of the drug. Images were acquired every 30 s for 30 min at varying zoom settings (1 to 3.5) using Zeiss AIM software and a 63 × 1.4 NA Zeiss Plan-Apochromat oil immersion objective.

Quantitation of Confocal Images—Three regions of 4 μm^2 each were selected in each cell as follows: one in the cytoplasm, one in the cell membrane, and one in the nucleus, avoiding to the degree possible the selection of subcellular organelles such as Golgi or the nucleoli. Mean intensities of the GFP-tagged constructs in the selected regions were calculated using the Zeiss AIM software for the images at the different time points; the ratio of the intensities for membrane/cytoplasm and nucleus/(membrane + cytoplasm) was then calculated and normalized to the time 0 values. The increase in the membrane/cytoplasm ratio and/or the decrease in the nucleus/(membrane + cytoplasm) ratio indicates translocation. For each series of images presented, the mean ± S.E. of the maximal translocation for all of the replicate experiments for that assay condition is presented.

Chemistry—The DAG-lactone derivatives were synthesized according to previously published procedures (39). Melting points were determined on an MPA 100 OptiMelt automated melting point system (Stanford Research Systems) or a Mel-Temp II apparatus (Laboratory Devices, USA) and are uncorrected. Column chromatography was performed on a Teledyne Isco CombiFlash Companion instrument under gradient elution conditions with RediSep disposable flash columns. Analytical TLC was performed on Analtech Uniplates silica gel GF. ^{1}H NMR spectra were recorded on a Varian Unity Inova instrument at 400 MHz. Spectra are referenced to the solvent in which they were run (7.24 ppm for $CDCl_3$). Positive ion fast atom bombardment mass spectra (FAB-MS) were obtained on a VG 7070E-HF double-focusing mass spectrometer operated at an accelerating voltage of 6 kV under the control of a MASPEC-II data system for Windows (Mass Spectrometry Services, Ltd.). Either glycerol or 3-nitrobenzyl alcohol was used as the sample matrix, and ionization was effected by a beam of xenon atoms generated in a saddle-field ion gun at 8.0 ± 0.5 kV. Nominal mass spectra were obtained at a resolution of 1200, and matrix-derived ions were background-subtracted during data system processing. Full experimental details and characterization have been reported previously for **6a**, **6c**, and **8b-e** (40). Full characterization of novel DAG-lactones designated as compounds **6b**, **8a**, and **8f** is described below. NMR spectra for these compounds can be found in the supplemental material.

*(E)-(2-(Hydroxymethyl)-4-((1-methyl-1H-indol-3-yl)methylene)-5-oxotetrahydrofuran-2-yl)-methyl 3-isobutyl-5-methylhexanoate (**6b**)*—^{1}H NMR (400 MHz, $CDCl_3$) δ 7.94 (t, J = 2.6 Hz, 1H, Ar), 7.82 (dt, J = 7.8, 0.9 Hz, 1H, Ar), 7.38 to 7.24 (m, 4H, Ar and C = C*H*), 4.31 (Ab q, J = 11.9 Hz, 2H, CH_2), 3.85 (s, 3H, CH_3), 3.77 (AB q, J = 12.1 Hz, 2H, CH_2), 3.06 (dd, J = 17.2, 2.7 Hz, 1H, CH_{4a}), 2.84 (dd, J = 17.1, 2.6 Hz, 1H, CH_{4b}), 2.22 (d, J = 6.5 Hz, 3H, CH_2 and O*H*), 1.90 (app sept, 1H, C*H*), 1.63 to 1.48 (m, 2H, 2 × C*H*), 1.17 to 0.96 (m, 4H, 2 × CH_2), 0.83 (dd, J = 6.6 Hz, 3H, CH_3), 0.82 (dd, J = 6.6 Hz, 6H, 2 × CH_3), and 0.78 (d, J = 6.6 Hz, 3H, CH_3); FAB-MS (*m/z*, relative intensity) 456 (MH^+, 97), 455 (M^+, 100).

*(E)-4-((5-(Hydroxymethyl)-2-oxo-5-((2-propyl-pentanoyloxy)methyl)dihydrofuran-3(2H)-ylidene)methyl)-1-propylpyridinium Bromide (**8a**)*—^{1}H NMR (400 MHz, $CDCl_3$) δ 8.88 (d, J = 6.7 Hz, 2 H, Ar), 8.16 (d, J = 6.6 Hz, 2 H, Ar), 7.66 (s, 1 H, C = C*H*), 4.74 to 4.56 (m, 2 H, CH_2), 4.33 (s, 2 H, CH_2), 3.94 (d, J = 12.0 Hz, 1 H, H_{4a}), 3.92 (AB q, J = 15.8 Hz, 2 H, CH_2), 3.73 (d, J = 12.0 Hz, 1 H, H_{4b}), 2.56 (v br s, 1 H, O*H*), 2.34 (tt, J = 8.8, 5.4 Hz, 1 H, C*H*), 2.02 (heptet, J = 7.4 Hz, 2 H, CH_2), 1.60 to 1.46 (m, 2 H, CH_2), 1.43 to 1.32 (m, 2 H, CH_2), 1.23 (m, 4 H, 2 × CH_2), 0.98 (t, J = 7.4 Hz, 3 H, CH_3), 0.86 (td, J = 7.3, 1.6 Hz, 6 H, 2 × CH_3); FAB-MS (*m/z*, relative intensity) 404 (M^+, 100).

*(E)-3-((5-(Hydroxymethyl)-5-((3-isobutyl-5-methylhexanoyloxy)methyl)-2-oxodihydro-furan-3(2H)-ylidene)methyl)-1-pentyl-pyridinium Bromide (**8f**)*—MP was 142–143 °C. ^{1}H NMR (400 MHz, $CDCl_3$) δ 9.76 (s, 1 H, Ar), 8.77 (d, J = 5.7 Hz, 1 H, Ar), 8.72 (d, J = 8.1 Hz, 1 H, Ar), 8.08 (irr t, 1 H, Ar), 7.39 (s, 1 H, C = C*H*), 4.89 (br s, 2 H, CH_2), 4.19 (AB q, J = 12.3 Hz, 2 H, CH_2), 3.73 (AB q, J = 12.3 Hz, 2 H, CH_2), 2.88 (dd, J = 18.6, 2.4 Hz, 2 H, H_{4ab}), 2.19 (d, J = 6.5 Hz, 2 H, CH_2), 2.04 (br s, 2 H, CH_2), 1.88 (irr sept, 1 H, C*H*), 1.55 (sept, J = 6.7 Hz, 2 H, 2 × C*H*), 1.38 to 1.35 (m, 4 H, 2 × CH_2), 1.15 - 0.94 (m, 4 H, 2 × CH_2), 0.92 to 0.75 (m, 15 H, 5 × CH_3); FAB-MS (*m/z*, relative intensity) 474 (M^+, 100).

Molecular Modeling—Structures for the single- and multiple site mutants of the Vav1 and PKCδ C1 domains were built by replacing residues while keeping their side chain χ angles as

close as possible to the conformation in the other structure. For example, in the Vav1 crystal structure (15), residue Glu^{9} has the conformation $\chi_1 = -74.7$, $\chi_2 = 166.2$, and $\chi_3 = 103.1$. When the M9E mutant of PKCδ was built, the Glu residue was rotated into the same conformation. In almost all cases, this conformation fit well into the structure, and the only exception was the P11T mutation in PKCδ, which required an adjustment of Leu^{20} and Phe^{13} to accommodate the threonine methyl group. This construction method allowed the structure of the mutated Vav1 C1 domain to be as similar as possible to the PKCδ C1b domain and vice versa.

Docking of phorbol and the DAG-lactones was performed using the software program GOLD Version 5.0 (41). The structure of phorbol 13-acetate was extracted from its co-crystal with the PKCδ C1b domain (7), and the C1 domain of Vav1 (15) was clipped from the larger structure. Hydrogens were added to both protein and ligands. The binding site was defined by atoms within a 10.0-Å sphere around the Nϵ atom of residue Gln^{27} (Gln^{542}(B) in the full-length structure). Ligand flexibility flags included internal hydrogen bond detection and ring corner flipping, and the default torsion angle distributions were used. The GoldScore scoring function was used with the default parameter file. The genetic algorithm settings were automatically optimized according to ligand flexibility with the search efficiency set to 100%.

After docking, the structures of the DAG-lactone-triple mutant PKCδ complexes were subjected to conformational searching using MacroModel (42) to identify low energy conformers for the charged ligand and protein side chains. The searches used 50 steps of systematic torsional sampling for each rotatable bond in the DAG-lactone *sn*-1 and *sn*-2 side chains, and in the side chains of residues Glu^{9}, Glu^{10}, and Thr^{11} in the mutated C1 domain. Minimization of each conformer found was done using the OPLS 2005 forcefield with octanol implicit solvent. All atoms in the DAG-lactone and residues 9–13, 20–24, and 27 in the binding site were free to move during minimization and the rest of the protein was held fixed.

Lipophilicity analysis was performed using the software program VASCo (43). The molecular lipophilicity potential over the surface of the protein was calculated in the following way. First, an atomic logP value was assigned to each atom. The atomic logP (AlogP) values used were those from Ghose *et al.* (44), although the dictionary provided with the VASCo program was modified to use the ionized forms of Asp, Glu, Arg, and Lys. Next, the solvent-excluded surface was constructed using MSMS (45), which yielded a set of surface vertices and triangles. Finally, the lipophilicity of each surface point was calculated using a Fermi-type distance function to map and smooth the logP value of nearby underlying atoms onto the surface, according to the formulation of Heiden *et al.* (46) for large molecules. The overall molecular lipophilicity potential (MLP) of the binding site area was calculated as the sum of the surface point lipophilicities for those points whose closest underlying atom lies on the solvent-accessible surface of the C1 domain in the region that inserts into the membrane and interacts with phorbol (7). This included the following atoms: residue 8, atoms O and Cα; residue 9, all atoms; residue 10, all atoms; residue 11, all atoms; residue 12, atoms N and Cα; residue 20, all atoms; residue 21, atom O; residue 22, atoms O, Cα, Cβ, Cγ, and Cδ; residue 23, all atoms; residue 24, all atoms; and residue 27, atoms Cγ, Cδ, and Nϵ.

RESULTS

Isolated C1 Domain of Vav1 Does Not Bind Phorbol Esters, Despite Conservation of the Appropriate Geometry of the Binding Pocket—The striking structural resemblance between the binding cleft of Vav1 C1 and that of PKCδ C1b, as revealed by recent x-ray crystallographic data (15), suggests the potential for preserved DAG/phorbol ester responsiveness of Vav1 (Fig. 1*B*). To confirm the ability of the Vav1 C1 domain binding site to accommodate phorbol ester, we extracted the phorbol 13-acetate ligand from the crystal structure of PKCδ C1b (7) and docked it into the isolated C1 domain from the highest resolution Vav1 crystal structure (15). As expected based on the structural overlay of the binding sites, phorbol ester is predicted to be able to bind to the Vav1 C1 domain with essentially the same binding mode as in the PKCδ C1b domain (Fig. 1, *C* and *D*). The binding site residues that form direct hydrogen bonding interactions with phorbol are identical between the two C1 domains, and the pattern of intra- and intermolecular hydrogen bonds formed by bound phorbol is preserved.

In contrast to this structural analysis and modeling, however, Vav1 has been shown experimentally not to interact with DAG or phorbol esters (18). One explanation for this apparent discrepancy could be that the C1 domain is located in the core of the Vav1 structure (rather than being exposed on the surface), and other structural domains prevent the access of ligands to the binding cleft. Examples of such masking of C1 domains, although in both instances not sufficient to fully block binding, are β2-chimerin (47) and PKCβ (48).

To test the possibility that the C1 domain is simply masked, we first cloned the isolated Vav1 C1 domain into a pGEX bacterial plasmid (Clontech) encoding a C-terminal GST tag and assessed the binding properties of the recombinant protein in an *in vitro* [^{3}H]PDBu binding assay. Compared with the GST-tagged PKCδ C1b (δC1b), a high affinity phorbol ester receptor that served as a positive control in these experiments, the Vav1 C1 showed no evidence for [^{3}H]PDBu binding even at very high (~1–2 μM) receptor concentration (data not shown) under these conditions.

Because misfolding of the purified protein from a bacterial expression system could be a reason for the absence of phorbol ester binding *in vitro*, we examined the phorbol ester responsiveness of the Vav1 C1 in the intracellular environment after eukaryotic expression. Phorbol ester causes the translocation of typical C1 domains to cellular membranes. We expressed a GFP-tagged Vav1 C1 in LNCaP cells, treated with phorbol ester, and looked for subcellular redistribution using real time confocal microcopy. The GFP-tagged C1b domain of PKCδ (δC1b-GFP) served as control, whose translocation dynamics had previously been extensively characterized by our laboratory (13, 49). After the administration of 1 μM PMA, δC1b-GFP showed a rapid but transient translocation into the cellular membrane, which was followed by translocation into the nuclear membrane (Fig. 5*A*). In contrast, PMA treatment failed to induce appreciable intracellular redistribution of Vav1

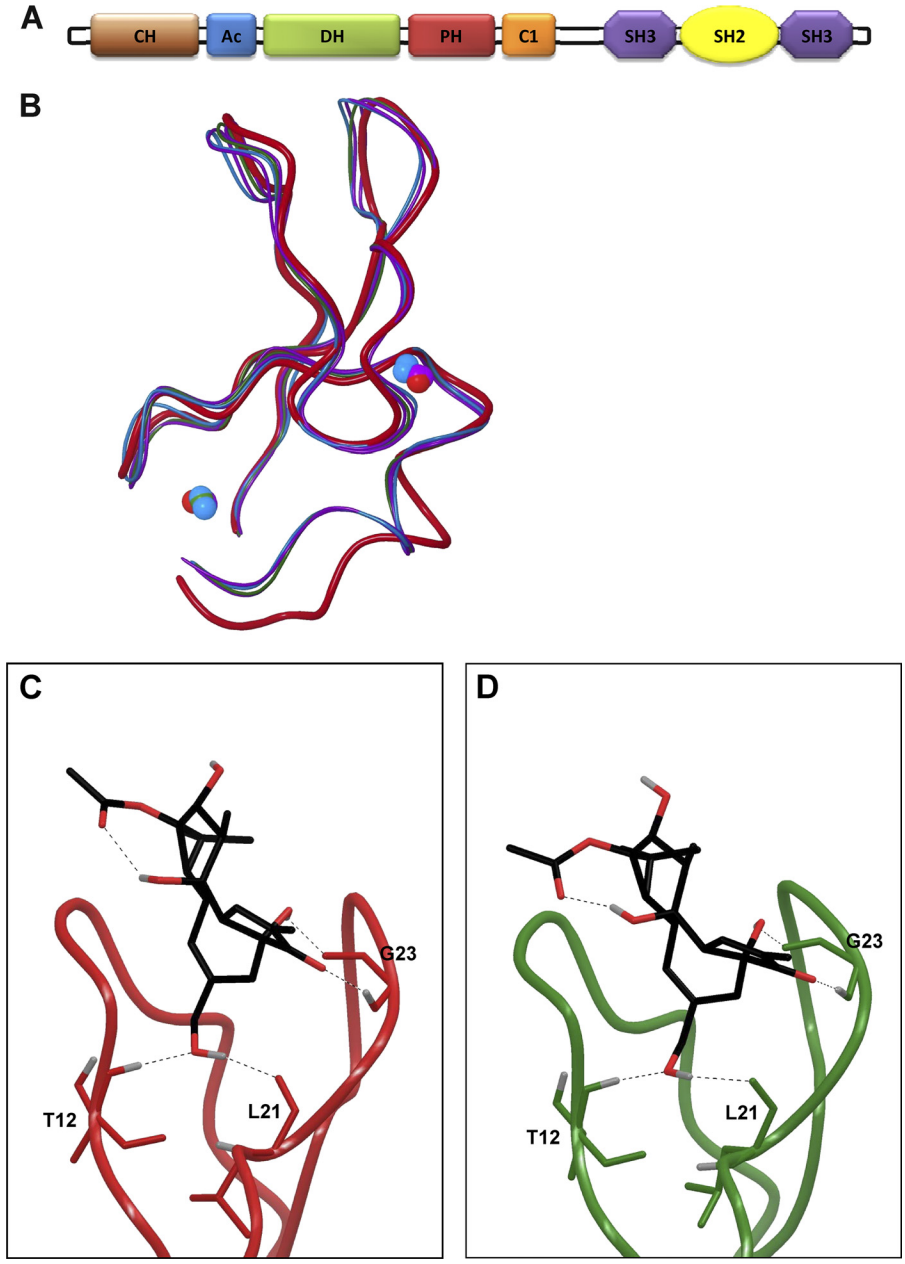

FIGURE 1. *A,* domain structure of the full-length Vav1. *B,* overlaid backbone structures of the C1 domain from PKCδ C1b in *red* (1PTR (7)), compared with the available structures for Vav1 in *green* (2VRW) (15), *blue* (3KY9) (14), and *purple* (3BJI) (16). The 3KY9 and 3BJI structures are both crystallographic dimers containing two copies of the C1 domain. Zinc atoms are rendered as CPK spheres. The backbone atoms of residues 231–274 in PKCδ are aligned to residues 516–559 in Vav1. The root mean square difference in these aligned atoms is ~0.5 Å between the Vav1 structures and PKCδ, and the root mean square difference in their full C1 domain backbones is ~1.4 Å. The C1 domains of PKCδ and Vav1 differ in the tilt angle of the small C-terminal helix, but the phorbol/DAG-binding sites remain essentially identical, with the same spacing between the loops forming the sides of the site, although the position of the loops relative to the rest of the domain may be shifted slightly. *C* and *D,* docking of phorbol 13-acetate into the binding cleft of δC1b and that of Vav1 C1. *C,* binding mode of phorbol 13-acetate as observed in the PKCδ C1b crystal structure (7). *D,* docked position of phorbol 13-acetate in the binding site of Vav1 (15). Hydrogen bonds are indicated by *dashed lines*.

C1-GFP, in agreement with the *in vitro* phorbol ester binding assays (Fig. 5*B*).

Multiple reports suggest that C1 domains may show somewhat differential recognition of the endogenous ligand, *sn*-1,2-diacylglycerol, relative to phorbol ester (49–51). We therefore examined the ability of dioctanoylglycerol to induce translocation of the GFP-tagged PKCδ C1b and Vav C1 domains (Fig. 5*C*). Clear translocation of the PKCδ C1b domain was observed at 100 μM DOG, as expected (52, 53). In contrast, no significant translocation of the Vav C1 domain was observed. These results suggest that the Vav C1 domain is unresponsive either to phorbol ester or to diacylglycerol.

Sequence Alignment of Vav1 C1 with Phorbol-responsive (Typical) C1 Domains Reveals Unique Residues around the Binding Pocket—Because the Vav1 C1 domain fails to bind phorbol esters despite preservation of the binding cleft geometry, a plausible explanation is that individual residues situated along the rim of the binding pocket or in close proximity to it may interfere with ligand-receptor interactions by impeding contacts between the C1 domain and the membrane lipids,

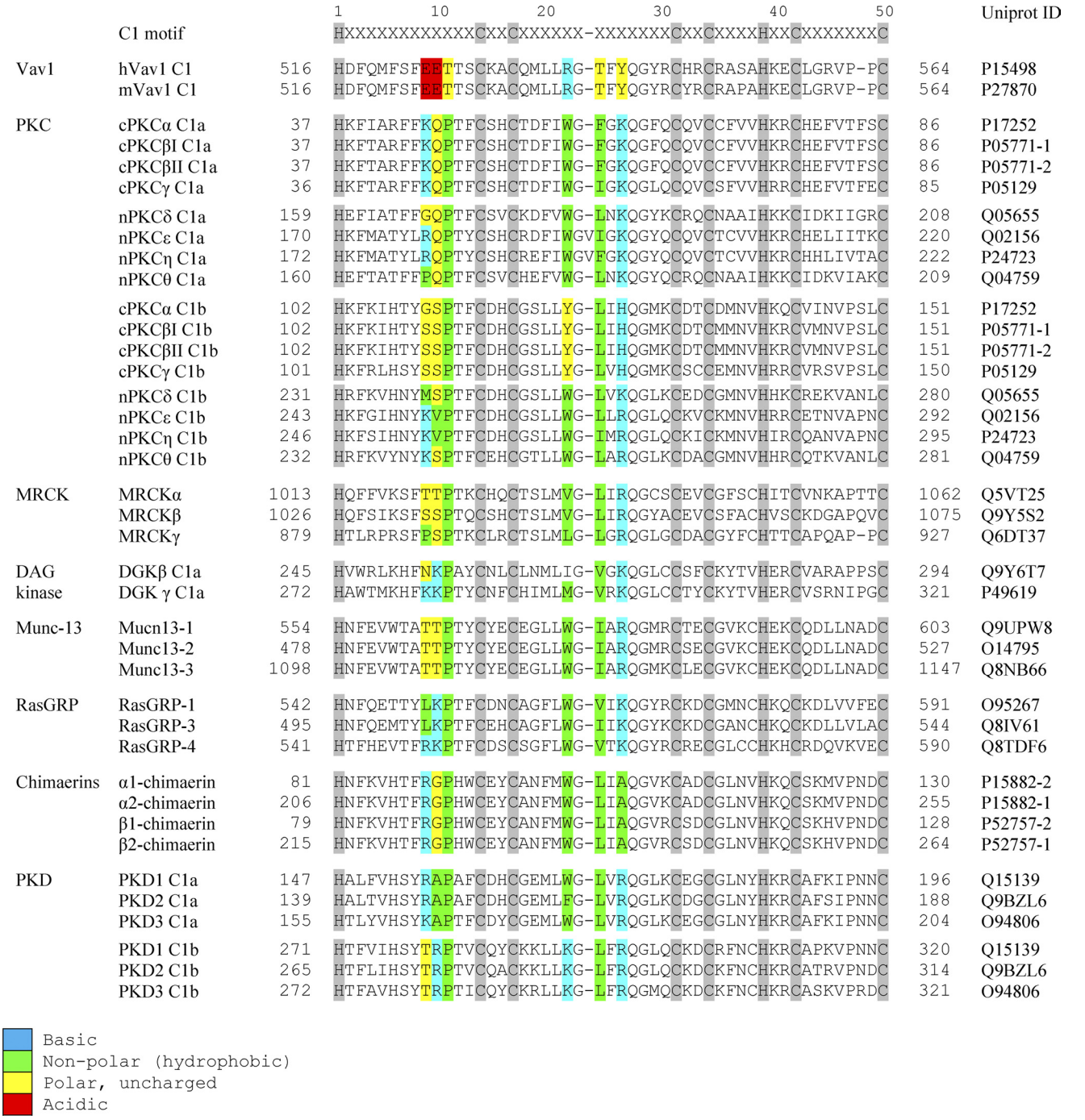

FIGURE 2. **Amino acid sequence alignment of the atypical C1 domain of Vav1 with all the members of the typical C1 domain-containing protein superfamily (human).** The positions in the C1 domains that were identified to be unique for the Vav1 structure are highlighted in *color*. The individual residues are categorized into four different groups based on their chemical properties: nonpolar (hydrophobic), polar uncharged, basic, and acidic. The *color code* is depicted in the *panel below* the sequences. The C1 consensus sequence is highlighted in *gray*.

thereby disrupting the ternary binding complex, or by occluding the binding site. This situation would thus be analogous to that of the atypical C1 domains of the aPKCs (13).

C1 domains consist of a conserved 50–51-amino acid sequence possessing the characteristic cysteine-rich motif $HX_{12}CX_2CX_nCX_2CX_4HX_2CX_7C$, where H is histidine, C is cysteine, *X* is any other amino acid, and *n* is 13 or 14 (Fig. 2, *gray-shaded letters*) (11). (In the text below, we will refer to residues using numbering internal to the C1 domain itself, to facilitate comparisons between C1 domains from different proteins. For example, the N-terminal histidine residue would be labeled His^{1}. This residue corresponds to His^{516} in full-length Vav1 and His^{231} in the C1b domain of full-length PKCδ.) A comprehensive sequence alignment of the atypical Vav1 C1 *versus* typical C1 domains highlighted several unique residues in the Vav1 C1 structure (Fig. 2). Six of these unique amino acids (Glu^{9}, Glu^{10}, Thr^{11}, Arg^{22}, Thr^{24}, and Tyr^{26}) are located at or close to the tip of the apparent binding cleft (see Fig. 3).

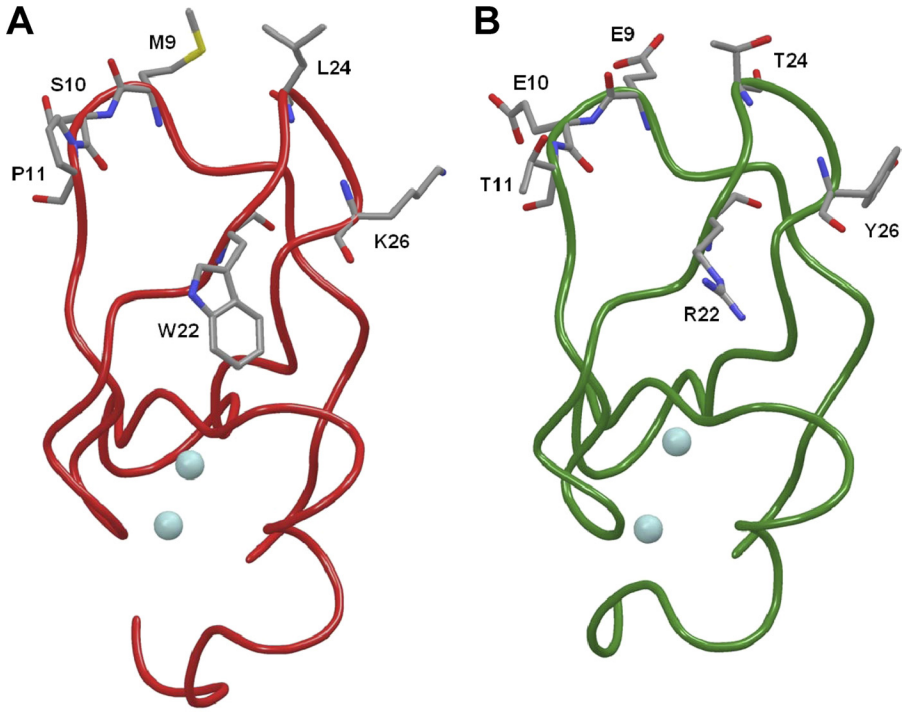

FIGURE 3. **Locations of the mutated residues in the C1 domains.** The locations of the residues subjected to mutation (*A*) in the PKCδ C1b domain (7) along the two loops forming the phorbol-binding site and the corresponding residues (*B*) in the Vav1 C1 domain (15) are shown.

Numerous studies indicate that hydrophobic residues exposed to the surface along the rim of the binding pocket of δC1b (at the tips of both loops forming the cleft: residues 9–12 in the N-terminal loop and 21–24 in the C-terminal loop) facilitate the insertion of the top third of the binding pocket into the membrane after ligand binding thereby stabilizing the formation of the ternary (ligand-receptor-membrane) binding complex (12, 54). The N-terminal loop of the binding pocket in Vav1 C1 contains two negatively charged Glu residues (Glu^9 and Glu^{10}) at the tip of the cleft. Although there is a moderate variability at these positions among typical C1 domains (see Fig. 2), acidic residues are not present in any of these sequences. In addition, the presence of Pro at position 11 is highly conserved among phorbol-binding proteins (Fig. 2), although the experimental evidence is not unambiguous regarding the role of Pro^{11} on binding potency (13, 55, 56). The C-terminal loop of the binding cleft (residues 20–27) contains three unique amino acids (Arg^{22}, Thr^{24}, and Tyr^{26}). With the exception of the C1b domains of protein kinase D isoforms, virtually all typical C1 domains contain highly lipophilic residues at the first two of these positions (positions 22 and 24) (Fig. 3), and the important role of Trp^{22} and Leu^{24} in the DAG/phorbol ester sensitivity of PKCδ has been well documented (7, 38, 56, 57). The third candidate in the C-terminal loop for disrupting the phorbol ester sensitivity of Vav1 C1 is Tyr^{26}. Almost every phorbol-sensitive C1 domain has a positively charged residue at this position (Arg^{26}, Lys^{26}, or His^{26}; see Fig. 2). According to the three-dimensional structure of δC1b, positively charged residues are exposed in the middle third of the C1 domain ("underneath" the top third of the cleft that is buried in the membrane) and interact with anionic phospholipid head groups (*e.g.* phosphatidylserine) in the membrane, thereby further strengthening the C1 domain-membrane interaction (7). Among the basic residues of δC1b, Lys^{26} is situated with closest proximity to the apex of the binding pocket (Fig. 3); therefore, it is a good candidate for such interactions between the C1 domain and acidic phospholipids. Tyr^{26} in Vav1 C1, being a noncharged residue, would have a reduced capacity to interact with acidic phospholipids.

Characterization of the Phorbol Ester Sensitivity of PKCδ C1b Mutants Possessing Vav1-C1-like Mutations

Single Site δC1b Mutants Demonstrated Only Moderate Decreases in the Binding Affinity for PDBu in Vitro—To determine the possible effect of the above unique residues on the ligand sensitivity of Vav1 C1, our initial approach was to use the C1b domain of PKCδ as a template and to mutate individual residues to the corresponding residues of Vav1-C1 at these positions (site 9, 10, 11, 22, 24, and 26). We first generated six single site C1b mutants fused to GST and determined their apparent [^{3}H]PDBu binding affinities (Table 1). Five out of six single site mutations (M9E/S10E/P11T/L24T/K26Y) caused a moderate decrease in the binding affinity of δC1b for [^{3}H]PDBu, whereas the W22R mutation had no effect on its potency for the ligand.

Replacement of the highly hydrophobic Met^9 residue with a negatively charged hydrophilic Glu^9 resulted in an 11-fold reduction in the binding affinity for [^{3}H]PDBu (K_d = 2.11 ± 0.11 nM). The introduction of Glu^{10} to replace the polar but uncharged Ser^{10} caused a 9.2-fold loss of measurable binding (K_d = 1.77 ± 0.06 nM), comparable with that of the previous mutation. These results suggest that, although the presence of an acidic residue at these sites decreases the binding potency by 1 order of magnitude, it does not abrogate the interactions

TABLE 1

***In vitro* binding affinities of [^{3}H]PDBu for WT δC1b and the single and multiple site δC1b mutants**

Individual C1 domains were fused with GST and expressed in a bacterial system and isolated, and the binding of [3H]PDBu to the individual C1 domains was measured. Values represent the mean ± S.E. (n = 3 independent experiments). NA means no activity.

Receptor (PKCδ C1b)	K_d	Relative to WT
	nM	
Wild type	0.193 ± 0.005	1×
Single mutants		
M9E	2.11 ± 0.11	10.9×
S10E	1.77 ± 0.06	9.1×
P11T	1.76 ± 0.21	9.1×
W22R	0.16 ± 0.02	0.8×
L24T	2.63 ± 0.15	13.6×
K26Y	0.97 ± 0.10	5.0×
Multiple mutants		
M9E/S10E	50.5 ± 2.1	261×
M9E/S10E/P11T	186.1 ± 6.0	963×
L24T/K26Y	96 ± 18	499×
M9E/S10E/P11T/ L24T/K26Y	NA	NA

within the ternary binding complex, because both the M9E and S10E mutants still retain a considerable potency for [^{3}H]PDBu.

The P11T mutant showed a 9.1-fold weaker affinity for [^{3}H]PDBu (K_d = 1.76 ± 0.21 nM) compared with the wild-type δC1b. Although the replacement of the nonpolar Pro residue with a polar Thr decreased the binding affinity (to the same degree as the glutamate mutations M9E and S10E), the relatively high residual potency of the P11T mutant argues that a threonine residue at this site is compatible with a significantly high level of phorbol ester affinity. This result is in good agreement with previous studies, which demonstrated that the replacement of Pro^{11} with arginine caused only a weak (4.4-fold) reduction in the binding potency of δC1b for [^{3}H]PDBu (13), comparable with the results obtained with the P11T mutant in this study.

The mutation at Trp^{22} had no effect on the phorbol ester binding of δC1b. The K_d value of the W22R mutant (0.16 ± 0.02 nM) remained essentially on the same level as that of the wild-type δC1b (0.193 ± 0.005 nM). This result agrees with our previous findings, which showed only a very weak reduction in the phorbol ester binding potency of δC1b after the introduction of Lys into this site (38). Therefore, we can conclude that, although almost every typical C1 domain (with the exception of some PKD isoforms) conserves a hydrophobic residue at site 22, the presence of positively charged residues at this site generally seems to be fully compatible with a high level of binding affinity, at least for phorbol esters. In contrast with the results for PDBu binding, binding of DAG has been described as being highly dependent on the presence of Trp^{22} (38, 57, 58).

Mutations at Leu^{24} (L24T) and Lys^{26} (K26Y) caused a similar decrease in binding affinity as did the other consequential mutations. Although our sequence alignment found that a polar residue (like Thr^{24}) essentially never occurs at position 24 for typical C1 domains (suggesting a crucial structural role for nonpolar residues), the influence of a polar residue at position 24 is thus apparently limited. Likewise, whereas the presence of a basic residue at site 26 is an almost uniform characteristic of typical C1 domains (with chimaerins being the sole exceptions), mutating the Lys^{26} of δC1b to a noncharged Tyr residue (to correspond to Vav1 C1) had only a modest effect.

We conclude that none of the unique residues (identified by our sequence alignment) in the Vav1 C1 structure by itself account for the lack of phorbol ester affinity. Rather, our results suggest that the loss of binding reflects the cumulative effect of multiple changes, each with more modest effect.

Combination of the Five Vav1-like Mutations in δC1b Resulted in a Dramatic Reduction in the Binding Affinity for PDBu in Vitro—To explore the combined effect of the above mutations on ligand sensitivity, we generated double, triple, and quintuple δC1b mutants (see Table 1) that contained multiple Vav1 C1-like residues in the same construct. Because the single site mutation at Trp^{22} had no effect on the binding affinity of δC1b for phorbol esters, we omitted this mutation from further study. As shown in Table 1, the double mutations at the apex of both loops of the binding cleft caused a considerable loss of binding affinity, with the L24T/K26Y mutant (C-terminal loop) showing a somewhat more pronounced reduction in its binding potency compared with that of the M9E/S10E mutant at the N-terminal loop. Except in the case of mutants including P11T, the reductions in binding affinities of the combined mutants were greater than the product of the reductions of the individual mutants. These results argue that the combined effect of multiple mutations on the binding affinity cannot be readily predicted based merely on the affinity results of single site mutants. Finally, the combined introduction of all five mutations (M9E/S10E/P11T/L24T/K26Y) into δC1b abolished detectable binding affinity. Under our *in vitro* assay conditions, this would imply a decrease of more than 5 orders of magnitude in binding potency (*i.e.* the mutated δC1b would not be able to bind [^{3}H]PDBu in the 10 μM range).

We conclude that the five unique residues Glu^9, Glu^{10}, Thr^{11}, Thr^{24}, and Tyr^{26} in the binding pocket of Vav1 are together sufficient to account for the lack of detectable phorbol ester binding activity by the Vav1 C1 domain. Studies described below will address the question of whether other residues in the Vav1 C1 domain further contribute to the lack of measurable phorbol ester binding.

The translocation experiments had provided no support for the suggestion that the Vav1 C1 domain could respond to diacylglycerol, despite its lack of response to phorbol ester. Although we could not measure binding of diacylglycerol to the Vav1 C1 domain directly, we could approach this question by examining the binding of DOG to several of our multiple site δC1b mutants that still retained some affinity for phorbol ester. The multiple site δC1b mutants in fact showed substantially decreased affinities for DOG, although the decreases in affinity were somewhat less than seen for [^{3}H]PDBu (Table 2).

Five Vav1-like Mutations in δC1b Modestly Influence the Phospholipid Selectivity of the C1 Domain—As described above, the five unique residues would be predicted to influence the interaction of the C1 domain with the phospholipid bilayer. For example, Sossin and co-workers (53) described a role for positively charged residues at positions 9, 10, and 26 of PKC Apl II from *Aplysia* in the recognition of phosphatidylserine and phosphatidic acid. We therefore examined the binding of [^{3}H]PDBu to wild-type PKCδ C1b and the double mutants

TABLE 2

***In vitro* binding affinities of DOG for WT δC1b and multiple site δC1b mutants**

Individual C1 domains were fused with GST and expressed in a bacterial system and isolated, and the binding of DOG to the individual C1 domains was measured by competition with [^{3}H]PDBu. Values represent the mean ± S.E. (n = 3 independent experiments).

Receptor (PKCδ C1b)	K_i	Relative to WT
	nM	
Wild type	22.3 ± 1.6	1×
M9E/S10E	1337 ± 247	60×
M9E/S10E/P11T	11,700 ± 3800	524×
L24T/K26Y	3870 ± 810	174×

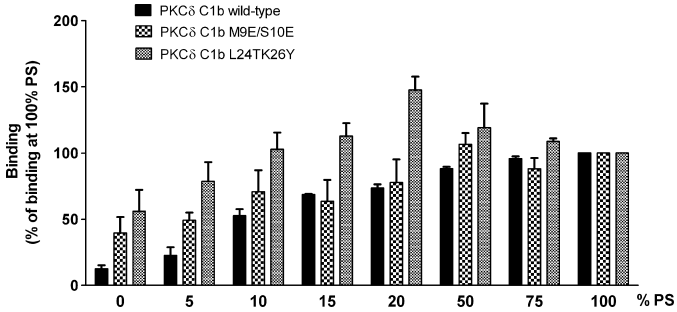

FIGURE 4. **Binding of [^{3}H]PDBu to wild-type δC1b and the double mutants δC1b M9E/S10E and δC1b L24T/K26Y was measured in the presence of phospholipid mixtures of PS/PC in the indicated proportions at 100 μg/ml of total phospholipid.** Values were expressed relative to binding in the presence of 100% PS. Data are the mean of triplicate experiments. *Bars,* ± S.E.

TABLE 3

***In vitro* binding affinities of [^{3}H]PDBu for WT δC1b and multiple site δC1b mutants**

Binding of [3H]PDBu was measured in the presence of a phospholipid mixture of 5% PS, 95% PC (100 μg/ml total phospholipid). Values represent the mean ± S.E. (n = 3 independent experiments.

Receptor (PKCδ C1b)	K_i
	nM
Wild-type δC1b	1.51 ± 0.25
δC1b M9E/S10E	180 ± 30
δC1b L24T/K26Y	360 ± 140

M9E/S10E and L24T/K26Y in the presence of PS/PC phospholipid mixtures with 100 μg/ml total lipid and variable proportions of PS (Fig. 4). Both pairs of mutations reduced the dependence on phosphatidylserine for [^{3}H]PDBu binding, as was most evident in lipid mixtures of 0–5% PS. In addition, the L24T/K26Y double mutant showed optimal binding at 20% PS, whereas the δC1b domain and the M9E/S10E double mutant bound best at 50–100% PS.

To better explore the basis for this difference in lipid selectivity, we determined the binding affinities for [^{3}H]PDBu of δC1b and the two double mutants in the 5:95 PS/PC lipid mixture. All three C1 domain showed reduced affinity but the loss of affinity was modestly greater in the case of the δC1b wild-type (Table 3). We conclude that the mutations causing the δC1b to more resemble Vav1 indeed influenced its lipid recognition. The change in lipid environment did not increase the binding affinity, however, arguing that the specific phospholipid composition was not responsible for the lack of the binding of the Vav1 C1 domain *in vitro*.

As a further control, we examined the ability of the wild-type Vav1 C1 domain to bind [^{3}H]PDBu in the presence of the 5:95 PS/PC lipid mixture. The experiments again failed to reveal binding of appreciable affinity, although under our conditions we cannot exclude affinities in the millimolar range (data not shown).

In Vivo Membrane Translocation Kinetics of GFP-tagged Multiple Site Mutants of δC1b Mirror Their Binding Activities Measured in Vitro—To explore how these mutations affect the phorbol ester response of δC1b in the intracellular environment, we investigated the plasma membrane translocation dynamics of the GFP-tagged δC1b mutants in LNCaP cells after the administration of various concentrations (0.1–10 μM) of PMA. Representative images for selected experiments are illustrated, but we also include quantitation for the multiple replicates under each experimental condition. In response to 1 μM PMA, the WT δC1b translocated rapidly to the plasma membrane, with loss from both the cytosol and nucleus (Fig. 5*A*). The redistribution of the signal from the cytosol into the plasma membrane was complete within 5–7 min after the application of PMA (data not shown), whereas the nuclear redistribution culminated after 10–15 min. Subsequently, the fluorescent signal began to return to the cytosol within 15–20 min and was clearly detectable at 30 min. The translocation dynamics of the wild-type molecule showed a clear dependence on the concentration of PMA. Reducing the concentration to 0.1 μM delayed the rapidity of translocation. Fig. 5*A* shows weak signs of plasma membrane translocation at 2–5 min, which became complete only after 15 min (in clear contrast to the 1 μM PMA treatment). However, increasing the concentration of the PMA treatment accelerated the translocation process. A very rapid and complete plasma membrane translocation of the WT δC1b with 10 μM PMA is visible within 2 min after activation, along with signs of nuclear membrane translocation (data not shown). Moreover, the return of the fluorescent signal into the cytosol began earlier than for the 1 μM treatment (at 10–15 min). The results obtained with the δC1b demonstrate that the translocation pattern was indicative of the concentration of PMA in this concentration range. Likewise, the δC1b domain translocated quickly after addition of DOG (100 μM) mainly to internal membranes with some plasma membrane translocation (Fig. 5*B*).

The double mutant M9E/S10E, which displayed a 260-fold reduction of potency compared with the wild-type δC1b in the above *in vitro* experiments, showed a much weaker response to 0.1 and 1 μM PMA (Fig. 5*A* and data not shown for 0.1 μM PMA). Increasing the concentration of the PMA to 10 μM resulted in a much faster response of M9E/S10E (Fig. 5*A*), similar in pattern to that obtained with the wild-type form after the application of 0.1 μM PMA as follows: (*a*) signs of plasma membrane translocation detected as early as 2 min; (*b*) more pronounced although incomplete translocation into the plasma membrane at later time points; and (*c*) redistribution of M9E/S10E from the nucleus within 20–30 min. The other double mutant (L24T/K26Y) displayed a very similar translocation pattern to M9E/S10E in response to PMA treatment. These results are consistent with the 260-fold (for M9E/S10E) and 498-fold (for L24T/K26Y) reductions in potency compared with WT δC1b *in vitro*.

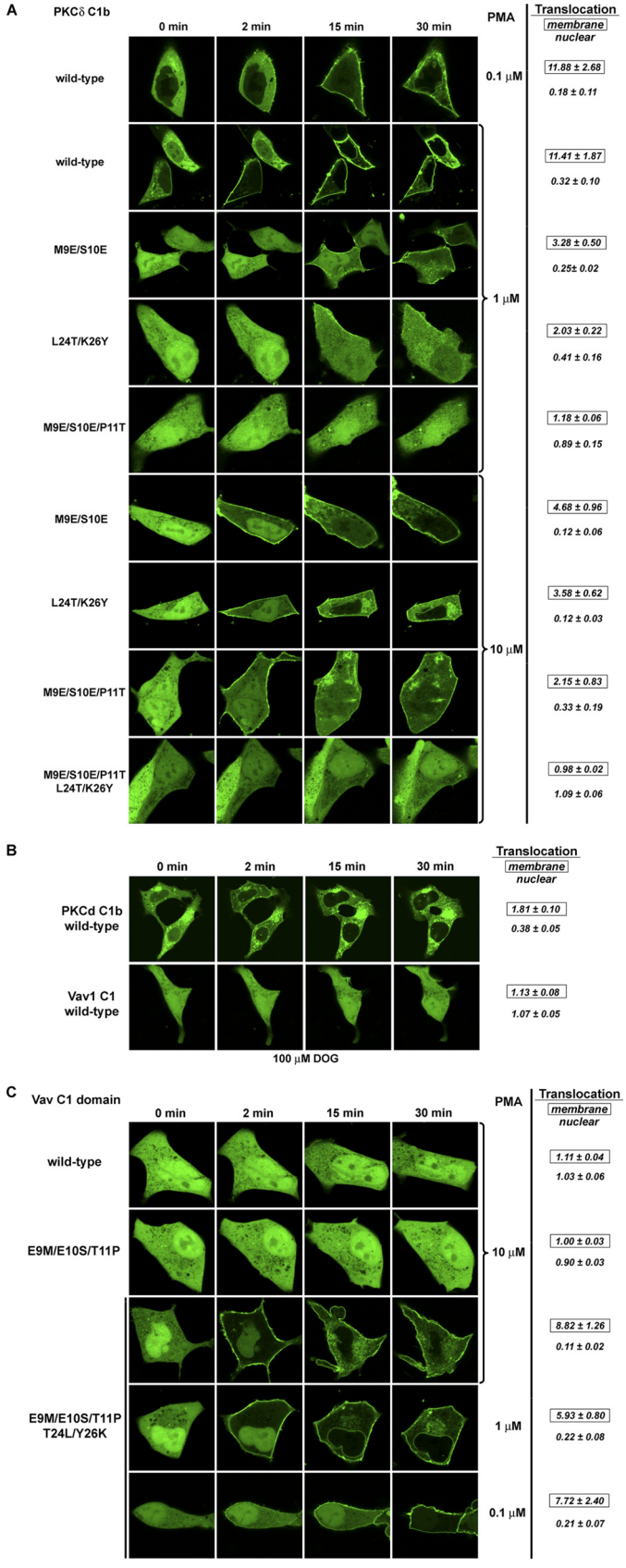

FIGURE 5. **Translocation pattern of the GFP-tagged wild-type δC1b and the multiple site mutants of δC1b in living LNCaP cells after PMA or DOG treatment.** Cells expressing the wild-type δC1b or the various multiple site mutants of δC1b were treated with PMA or DOG. The translocation pattern was examined by confocal microscopy as a function of time. Pattern of translocation was in response to *A*. PKCδ C1b wild-type and the multiple site mutants were treated with PMA (0.1–10 μM). *B*, PKCd C1b wild-type and Vav1 C1 wild-type treated with 100 μM DOG. *C*, Vav1 C1 wild-type and the multiple site mutants treated with PMA (0.1–10 μM). Each *panel* represents images typical of three to six independent experiments. Maximal extents of translocation, measured as the increase in the ratio of plasma membrane/cytoplasmic staining (designated *membrane*) or as the decrease in the ratio of nuclear/(cytoplasm and plasma membrane) staining (designated *nuclear*) were quantitated for all replicates and presented as the mean ± S.E.

The triple mutant (M9E/S10E/P11T) showed a more severe loss of binding potency for [^{3}H]PDBu *in vitro*, compared with that of the double mutants (963-fold reduction). In agreement with this, the triple mutant (M9E/S10E/P11T) showed a hardly detectable response to PMA at 1 μM (Fig. 5*A*). However, similar to the double mutants it did display a fairly quick response to 10 μM PMA (Fig. 5*A*), with detectable plasma membrane translocation as early as 2 min, and a partial translocation out of the interior of the nucleus at later time points (20–30 min). This confirms the severe reduction (960-fold) of binding potency that was measured *in vitro* but also demonstrates that, similar to the *in vitro* findings, a certain degree of phorbol ester response remained detectable for the triple mutant *in vivo* as well. In contrast to the double and triple mutants, we could not detect any signs of intracellular redistribution of the quintuple mutant (M9E/S10E/P11T/L24T/K26Y) in response to PMA at this concentration range (Fig. 5*A*). Increasing the concentration of PMA above 10 μM resulted in severe disorganization of the cellular architecture, so we were unable to explore possible translocation at higher PMA concentrations. We conclude that our *in vivo* translocation studies support the important contribution of the five unique residues along the rim of the binding pocket to the lack of phorbol ester affinity of Vav1 C1.

Characterization of the Phorbol Ester Sensitivity of Vav1 C1 Mutants Containing δC1b-like "Back" Mutations

Introduction of Five δC1b-like Mutations into the Sequence of Vav1 C1 Resulted in an Almost Complete Recovery of Phorbol Ester Sensitivity, Both in Vitro and in Vivo—Although the above studies argue that the five unique residues we identified in the Vav C1 domain could be sufficient to account for the loss of Vav1 phorbol ester binding, it is possible that other residues in the Vav C1 domain independently might also interfere with binding. To address this question, we generated a quintuple back-mutant of Vav1 C1 (E9M/E10S/T11P/T24L/Y26K), which contained the corresponding residues of δC1b at positions 9, 10, 11, 24, and 26 in the binding cleft but retained all the other native residues of Vav1. We evaluated the *in vitro* binding affinity of the GST-tagged quintuple back-mutant for [^{3}H]PDBu. Strikingly, it bound [^{3}H]PDBu and did so with high affinity (K_d = 1.05 ± 0.15 nM (Table 4), compared with K_d = 0.193 ± 0.005 nM for the wild-type δC1b (Table 1)). We conclude that the five residues identified are the primary basis for the failure of Vav1 to bind phorbol ester. An additional residue or residues must make a further minor contribution to affinity, accounting for the remaining 5-fold affinity difference.

The *in vivo* translocation experiments with the GFP-tagged quintuple back-mutant (E9M/E10S/T11P/T24L/Y26K) confirmed the phorbol ester responsiveness. In contrast to the

TABLE 4

K_d values of [^{3}H]PDBu for binding to wild-type Vav1 C1 and different multiple site Vav1 C1 mutants

GST-tagged C1 domains were expressed in a bacterial system and isolated, and the binding potencies for [3H]PDBu were determined. Values represent the mean ± S.E. (n = 3 independent experiments). NA means no activity.

Receptor (Vav1 C1)	K_d	Relative to PKCδ C1b WT	Relative to Vav1 C1 E9M/E10S/T11P/T24L/Y26K
	nM		
Wild type	NA	NA	NA
E9M/E10S	NA	NA	NA
T24L/Y26K	NA	NA	NA
E9M/E10S/T11P	7330 ± 490	38,000×	6985×
E9M/E10S/T11P/T24L/Y26K	1.05 ± 0.14	5.4×	1×
Quadruple mutants			
E10S/T11P/T24L/Y26K (−E9M)	980 ± 120	5052×	929×
E9M/T11P/T24L/Y26K (−E10S)	26.4 ± 2.4	137×	25.1×
E9M/E10S/T24L/Y26K (−T11P)	198 ± 18	1026×	189×
E9M/E10S/T11P/Y26K (−T24L)	34.9 ± 3.9	181×	33.2×
E9M/E10S/T11P/T24L (−Y26K)	31.4 ± 5.1	163×	29.9×

wild-type Vav1 C1, which showed no response to phorbol ester or DOG treatment, the quintuple back-mutant displayed translocation in response to as little as 0.1 μM PMA (Fig. 5*C*), reflecting high phorbol ester sensitivity comparable with that obtained with WT δC1b. In addition, the translocation kinetics/pattern of the quintuple Vav1 back-mutant, like that of the wild-type δC1b, showed a dose-dependent change on PMA concentration, *i.e.* increasing the concentration of PMA accelerated the process of plasma membrane translocation and that of nuclear translocation.

Collectively, the almost complete recovery of the binding affinity of Vav1 C1 E9M/E10S/T11P/T24L/Y26K (consistent with the results obtained with δC1b mutants) further support previous crystallographic results (15) and our docking results, which demonstrate a retained binding cleft geometry for Vav1 C1 and a conserved binding pocket for ligand interaction. The reason for the lack of ligand affinity is the presence of these five residues at the rim of the binding pocket which presumably hinder the association of the C1 domain with the cellular membrane, thereby destabilizing the ternary binding complex and reducing the potency for phorbol esters.

Introduction of Double-, Triple-, and Quadruple δC1b-like Mutations into the Sequence of Vav1 C1 Further Dissects the Role of the Individual Residues in the Ligand Affinity of Vav1 C1—To further explore whether all five residues actually contribute to the lack of binding potency in the WT Vav1 C1, we generated double, triple, and quadruple back-mutants of Vav1 C1 (see Table 4). Introducing two back mutations into the N-terminal (Vav1 C1 E9M/E10S) or the C-terminal (T24L/Y26K) loop of the apparent binding cleft of Vav1 C1 was insufficient to recover the phorbol ester response of the molecule. *In vitro* assays could not detect any measurable [^{3}H]PDBu binding (Table 4), and no translocation could be observed *in vivo* after 10 μM PMA treatment (data not shown). Back-mutating the three residues in the N-terminal loop (E9M/E10S/T11P) conferred only a very weak binding potency (K_d = 7330 ± 490 nM) on the triple back-mutant (Table 4), which could only be detected *in vitro* but not with translocation assays (data not shown). These results suggest that the presence of compatible residues at the tip of both loops is needed for appropriate binding affinity. They stand in partial contrast to the previous findings with the double (M9E/S10E; L24T/K26Y) and triple (M9E/S10E/P11T) mutants of δC1b (Table 1 and Fig. 5*A*), which failed to completely abolish the binding potency of the δC1b mutants. Because the difference lies in the presence of other residues in the PKCδ C1b domain *versus* Vav1, it emphasizes both that these residues make a difference and that the effects of the combination of residues are not simply additive.

Next, using quadruple back-mutants of Vav1 C1 (listed in Table 4), we analyzed the individual contribution of each of the five residues in the backbone structure of the Vav1 C1 to the lack of ligand binding, for comparison with their contributions in the context of the PKCδ C1 domain. In this set of experiments, the quintuple back-mutant of Vav1 C1 (E9M/E10S/T11P/T24L/Y26K) can be considered analogous to the WT δC1b (both containing the appropriate residues for potent ligand binding) and the quadruple back-mutants of Vav1 C1 (see Table 4) analogous to the single site mutants of δC1b (see Table 1) of our previous experiment (all possessing one residue less than required for the most potent binding cleft geometry). (For brevity we will refer to the quadruple back-mutants by mentioning the residue that they lack, compared with the quintuple Vav1 C1 mutant, with an antecedent negative sign; see Table 4 for details.) The binding constants (K_d values) of three out of five quadruple mutants showed a nearly uniform reduction in potency. The mutants (−E10S), (−T24L), and (−Y26K) all displayed a decrease of 25–35-fold in potency for [^{3}H]PDBu, compared with the binding affinity of the quintuple Vav1 C1 mutant (Table 4). This is consistent with the uniform reduction (5–13-fold; see Table 1) in the binding affinity of the single site δC1b mutants compared with their wild-type counterpart, although the degree of reduction is slightly higher than in the case of δC1b mutants. However, in contrast to the single site mutants of δC1b at site 9 and 11 (δC1b M9E and δC1b P11T), their analogous quadruple Vav1 C1 mutants (Vav1 C1 −E9M and −T11P, respectively) displayed a more severe reduction in their binding potencies (929-fold for −E9M and 189-fold for −T11P compared with the quintuple Vav1 C1 mutant). This suggests a more significant role for Met^9 and Pro^{11} in ligand binding within the backbone structure of Vav1 C1, as opposed to that observed in the context of δC1b. In agreement with the *in vitro* results, the *in vivo* translocation experiments with the quadruple back-mutants confirmed that Met^9 and Pro^{11} had a larger effect on phorbol ester response than did the other three residues (Ser^{10}, Leu^{24}, and Lys^{26}). As seen in Fig. 6, the application of 10 μM PMA induced a quick plasma membrane translo-

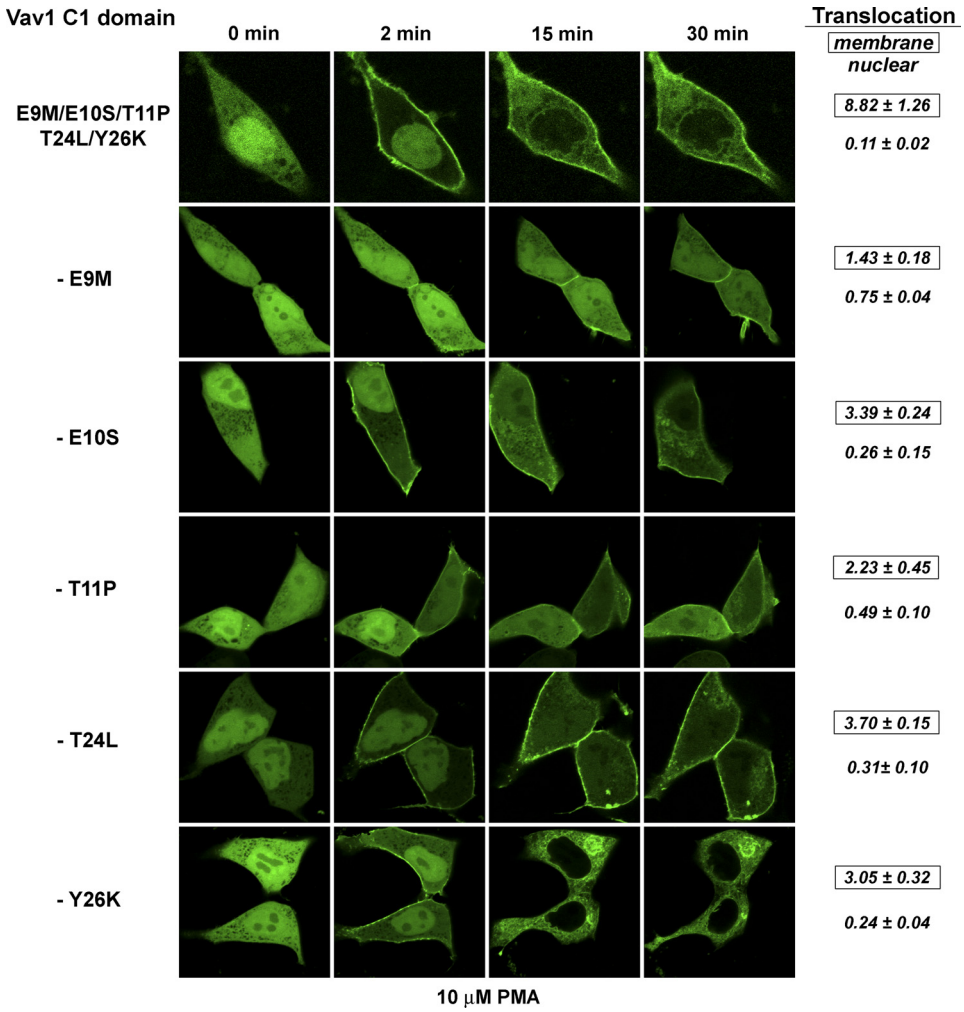

FIGURE 6. **Translocation pattern of the GFP-tagged quintuple and quadruple Vav1 C1 back-mutants in living LNCaP cells after PMA treatment.** Cells expressing the quintuple back-mutant Vav1 C1 E9M/E10S/T11P/T24L/Y26K and the indicated quadruple back-mutants were treated with 10 μM PMA. Cells were imaged by confocal microscopy, and images captured at the indicated times are shown. Each panel represents a typical image of three to five independent experiments. Maximal extents of translocation, measured as the increase in the ratio of plasma membrane/cytoplasmic staining (designated *membrane*) or as the decrease in the ratio of nuclear/(cytoplasm and plasma membrane) staining (designated *nuclear*) were quantitated for all replicates and presented as the mean ± S.E.

cation in the case of the −E10S, −T24L, and −Y26K mutants. In addition, although the redistribution from the cytosol into the plasma membrane was not complete, we could observe a fairly strong fluorescent signal in the membrane within 15 min after the administration of the drug, and an almost complete translocation out of the interior of the nucleus. In contrast, the −E9M mutant displayed only a weak translocation into the plasma membrane that had much slower kinetics than that of the previous three mutants and was limited to certain regions of the plasma membrane. Moreover, the nuclear translocation was also limited for this mutant. The translocation of the −T11P mutant in response to PMA displayed an intermediate pattern compared with that of the three more potent mutants (−E10S, −T24L, and −Y26K) and −E9M, which showed the weakest response. Although a fairly quick initial plasma membrane translocation could be detected, the redistribution from the cytosol was only partial, and the fluorescent signal was absent from certain regions of the plasma membrane. In addition, translocation out of the nucleus was quite limited.

Collectively, the results obtained with the quadruple Vav1 C1 mutants emphasize the prominent contribution of Met^{9} and Pro^{11} to the binding affinity of the quintuple Vav1 C1 mutant (E9M/E10S/T11P/T24L/Y26K) for phorbol esters, which in turn indicates that Glu^{9} and Thr^{11} make a more significant contribution to the reduction of the binding potency of the wild-type Vav1 C1, compared with the other three residues (Glu^{10}, Thr^{24}, and Tyr^{26}).

Rationalizing the Phorbol Binding and Membrane Translocation Behavior of PKCδ and Vav1 Mutants in Terms of Molecular Lipophilicity

A plausible interpretation of the role played by the five unique residues was that the lack of phorbol ester responsiveness in Vav1 was due to the inability of its C1 domain to associate with and insert into the membrane, forming the ternary protein + ligand + lipid complex that is required for successful ligand binding. To better assess this model, we developed a method of calculating and quantifying the differences in lipophilicity between our various C1 domain mutants. We were

interested in seeing how the membrane affinity of a C1 domain mutant correlated with its K_d value for PDBu and its membrane translocation behavior.

The standard metric for quantifying the hydrophobicity or lipophilicity of small molecules is logP, a measure of the partition coefficient between octanol and water. However, logP is a whole-molecule number and as such is not particularly useful for characterizing macromolecules, where the lipophilicity may vary significantly between different parts of the structure. This is especially true for peripheral membrane proteins such as the typical (DAG/phorbol-responsive) C1 domains. Computational methods for estimating logP generally involve summing up the fractional lipophilicities of individual atoms or small fragments. These values are based on regression analysis from libraries of small molecules with carefully measured experimental values of logP (44). The concept of an MLP is an extension of these types of calculations that can be applied to larger molecules such as proteins. The MLP is analogous to an electrostatic potential around a protein based on the partial charges on individual atoms. Each atom is assigned an atomic logP (AlogP) value, and these values are then projected outward from the underlying atoms onto the solvent-accessible molecular surface. In other words, the lipophilicity value at each point on the surface is a smoothed distance-dependent function of the fractional logP values of all nearby atoms (59). An algorithm for this calculation has been implemented in the software program VASCo (43), which also includes a plugin for PyMOL (60) for surface visualization.

We built model structures for each of the single and multiple site mutants of the Vav1 and PKCδ C1 domains and calculated the molecular lipophilicity potentials over their surfaces using VASCo. Fig. 7*A* shows a view of these surfaces, for the wild-type, triple, and quintuple mutant structures, seen from an orientation looking down into the binding site. The surfaces are colored according to the value of the lipophilicity at each point. The binding site surfaces for all the C1 domains are mainly of intermediate lipophilicity (green colored) with patches of stronger hydrophobicity (red color). Wild-type PKCδ is more lipophilic than wild-type Vav1, due mainly to the presence of Met^{9}, Pro^{11}, and Leu^{24}. Wild-type Vav1 has only one patch of strong hydrophobicity, at Leu^{20}. However, the presence of Glu^{9} and Glu^{10} does not introduce any strong hydrophilic character (blue color) to the binding site, as the polarity of the carboxylate groups is smoothed out by surrounding nonpolar atoms. Similarly, Arg^{22} in Vav1 does not appear significantly more hydrophilic than Trp^{22} in PKCδ, because its guanidinium headgroup lies folded down below the surface of the binding site, and it is the methylene groups in the side chain that form part of the rim. Thus, Fig. 7*A* offers a qualitative explanation of the relatively small effects of individual mutations and suggests that it is the overall lipophilicity of the top third of the C1 domain that drives its ability to respond to phorbol.

To look at the correlation between molecular lipophilicity and phorbol sensitivity, the sum of the MLP over the surface of the binding site for each of the PKCδ C1b and Vav1 C1 domain constructs was extracted from the VASCo output and is plotted in Fig. 7, *B* and *C*, along with the [^{3}H]PDBu binding affinities and a color-coded summary of translocation behavior. Translocation assays were not performed for all of the PKCδ C1b single mutants, but in those cases good phorbol binding affinity was assumed to imply a normal translocation response. At the two ends of the scale, it is clear that C1 domains with high lipophilicity on the binding site surface bind PDBu *in vitro* with good affinity and translocate *in vivo* in response to PMA; conversely, C1 domains with low binding site lipophilicity do neither of these things. Approximate cutoffs can be drawn to say that C1 domains with binding site MLP values >0.0 will be fully phorbol-responsive, C1 domains with binding site MLP values < -10.0 will not be phorbol-responsive, and C1 domains with binding site MLP values between 0.0 and -10.0 will probably retain some phorbol-binding ability but may or may not be fully responsive.

The quintuple mutated Vav1 C1 domain remains slightly less lipophilic than the wild-type PKCδ C1b domain, and conversely quintuple mutated PKCδ is still more lipophilic than wild-type Vav. This indicates that the five mutations do not completely manage to "convert" one C1 domain into the other, in terms of the overall lipophilicity, but they come quite close. The largest numerical part of the difference is due to Trp *versus* Arg at position 22, but as we have shown earlier, this substitution does not affect phorbol binding at all.

The K26Y and S10E single mutants of PKCδ and the corresponding Vav1 quadruple mutants −E10S and −Y26K show the smallest changes in lipophilicity relative to wild-type PKC and quintuple mutant Vav1. Thus, it is not surprising that these mutants retain strong phorbol binding affinities. In fact, Glu at position 10 is actually more lipophilic than Ser because of the methylene units in the side chain. As discussed above, position 26 is not directly involved in the binding site surface, because it is located below the binding site in the middle third of the C1 domain. However, Tyr at this position does slightly increase the lipophilicity of the surface near residues 8 and 9.

The other PKCδ single mutants and Vav1 quadruple mutants have intermediate lipophilicities, in roughly the same range as the double and triple mutants of PKCδ and the triple mutant of Vav1. In this intermediate range, phorbol binding affinities and translocation dynamics do not necessarily correlate linearly with the numerical MLP values. For example, the molecular lipophilicity calculations do not explain the stronger-than-expected negative effect of double mutations in PKCδ (or the triple mutation in Vav1, which is structurally equivalent to the PKCδ L24T/K26Y double mutant). An alternative interpretation of the data is that the Vav1 quadruple −T24L mutant as well as the PKCδ M9E and L24T mutants show much *better* phorbol responsiveness than would be expected based on their binding site lipophilicities. The difference between Thr and Leu at residue 24 gives a significant difference in the binding site MLP, yet this substitution on its own produces only a modest effect on phorbol binding, and the Vav1 −T24L mutant can translocate rapidly. It is interesting that this mutant does show an altered subcellular distribution, with a concentration in the nucleus, before phorbol is applied to the cells (Fig. 6). These results suggest that for C1 domains with intermediate lipophilicities, the ability to respond to phorbol may depend on the precise locations of hydrophobic and hydrophilic residues in

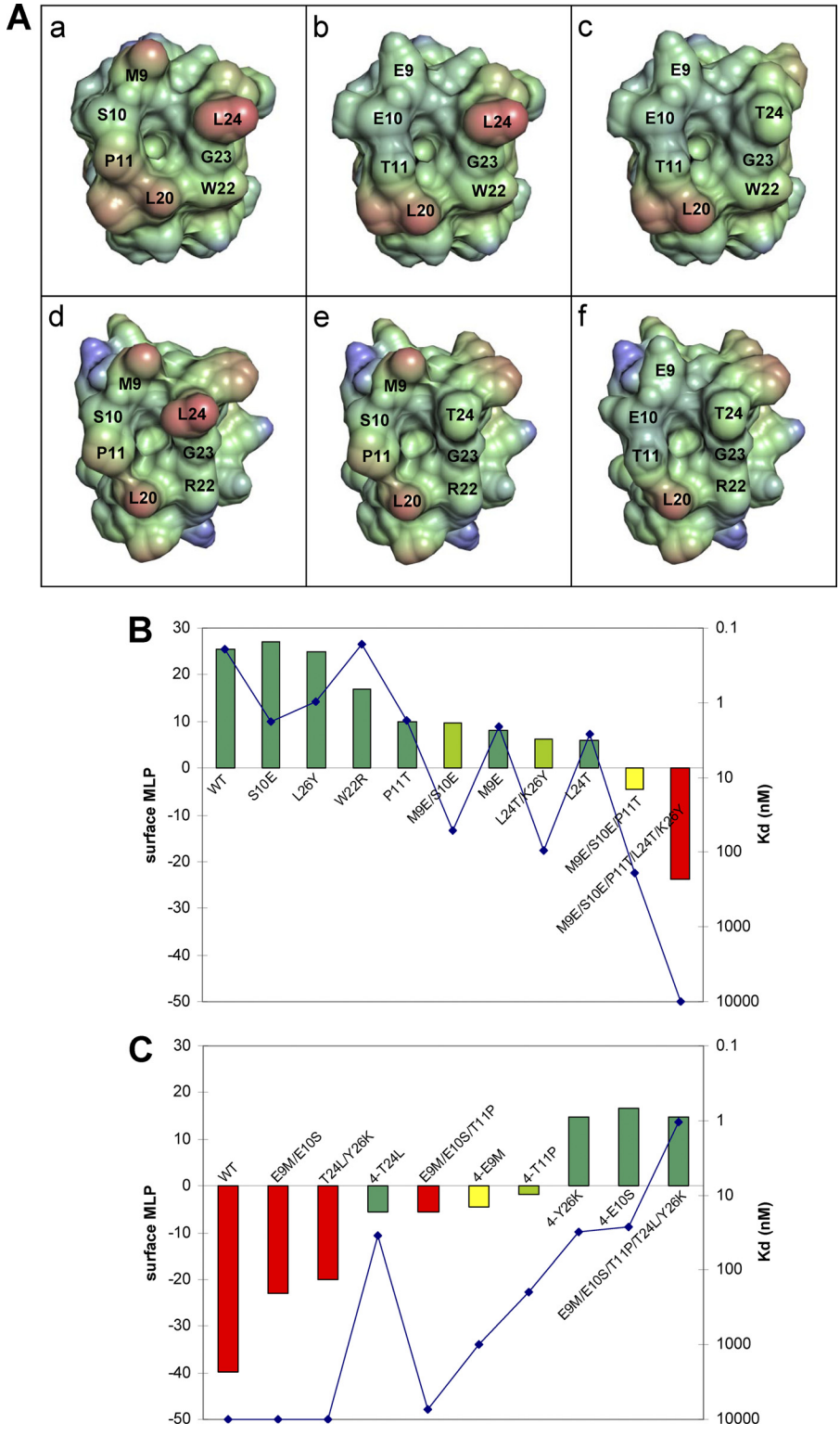

FIGURE 7. *A,* modeling of solvent-accessible surfaces of the C1 domain constructs. The surfaces of C1 domains are colored according to the molecular lipophilicity potential, from *blue* (hydrophilic) to *red* (lipophilic). *Panel a,* wild-type PKCδ C1b. *Panel b,* PKCδ C1b M9E/S10E/P11T. *Panel c,* PKCδ C1b M9E/S10E/P11T/L24T/K26Y. *Panel d,* Vav1 C1 E9M/E10S/T11P/T24L/Y26K. *Panel e,* Vav1 C1 E9M/E10S/T11P. *Panel f,* wild-type Vav1. Note that residue 26 is not visible in this orientation, which is looking down into the phorbol-binding site from the top of the domain. *B* and *C,* quantification of the overall molecular lipophilicity potential (*MLP*) of the membrane-interacting and phorbol-binding site area of the δC1b and Vav1 C1 domains (see "Experimental Procedures" for details on the MLP calculations). *B,* MLP (colored *bars*) for PKCδ C1b mutant constructs. The wild-type structure is on the *left*, and the mutants are arranged from most to least lipophilic. *C,* MLP for Vav1 C1 domain mutant constructs. The wild-type structure is on the *left*, and mutants are ordered from least to most lipophilic. The *bars* are colored *green* for C1 domains that translocate normally in response to PMA, *light green* for domains which translocate more slowly, *yellow* for domains that showed partial or limited translocation behavior, and *red* for domains that did not translocate at all or showed negligible translocation. The binding affinity to [^{3}H]PDBu for each C1 domain is plotted on the *right-hand axis* on a log scale (*blue points* and *line*).

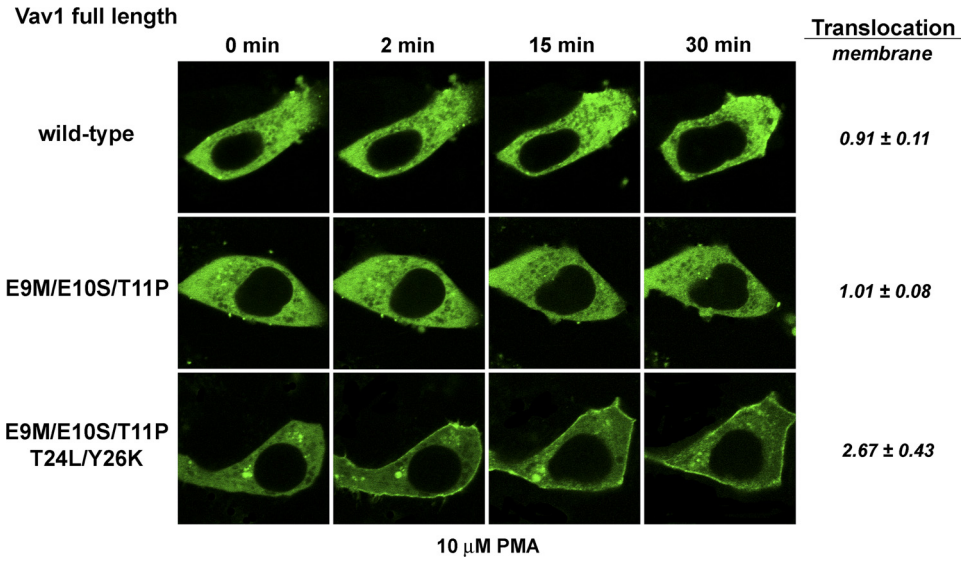

FIGURE 8. **Translocation pattern of the full-length versions of GFP-tagged wild-type Vav1 and the triple and quintuple Vav1 back-mutants in living LNCaP cells after PMA treatment.** Cells expressing the full-length proteins of the wild-type Vav1, of the triple back-mutant, and of the quintuple back-mutant were imaged by confocal microscopy after the application of 10 μM PMA. Images captured at the indicated times are shown. Each panel represents a typical image of four to six independent experiments. Maximal extents of translocation, measured as the increase in the ratio of plasma membrane/cytoplasmic staining (designated "membrane") were quantitated for all replicates and presented as the mean ± S.E.

the binding site, and the balance of lipophilicity across the C1 domain.

Quintuple Mutated C1 Domain of Vav1 Retains Its Phorbol Ester Sensitivity in the Context of the Full-length Molecule and Is Capable of Targeting the Protein to the Cellular Membrane in Response to Ligand

To elucidate whether the binding cleft of the Vav1 C1 is capable of interacting with phorbol esters in the context of the full-length molecule, we generated a full-length quintuple Vav1 back-mutant, which contained the same five back-mutations (E9M/E10S/T11P/T24L/Y26K) in its C1 domain as the quintuple mutant of the isolated Vav1 C1. We speculated that if the binding cleft is not occluded by other domains in the full-length molecule, the introduction of the five crucial residues into the C1 domain would confer phorbol ester sensitivity on the full-length Vav1 protein as well. We cloned the genes of the quintuple full-length mutant (Vav1 E9M/E10S/T11P/T24L/Y26K) along with its wild-type counterpart into a vector encoding an N-terminal GFP fusion tag, and we subjected them to *in vivo* translocation assays. (Because of technical difficulties with producing sufficient amounts of purified protein, we were unable to conduct *in vitro* binding experiments on full-length Vav1.) Fig. 8 shows that, similar to the findings with the isolated Vav1 C1, the full-length quintuple back-mutant of Vav1 (Vav1 E9M/E10S/T11P/T24L/Y26K) possessed affinity for phorbol esters, because the application of 10 μM PMA resulted in the translocation of the protein into the plasma membrane. In clear contrast with the quintuple Vav1 mutant, the wild-type and the triple mutant (Vav1 E9M/E10S/T11P) of the full-length Vav1 failed to redistribute from the cytosol into the plasma membrane (similar to the results obtained with the isolated Vav1 C1). These results demonstrate unambiguously that replacing the residues of Vav1 at positions 9–11, 24, and 26 (of its C1 domain) with δC1b-like amino acids confers phorbol ester sensitivity on the full-length Vav1 protein as well. In the context of the interaction of the C1 domain of Vav1 with the DH and PH domains (Fig. 9*A*), it can be seen that the three residues on the N-terminal loop point out into solvent. Thus, although mutating these three residues can provide some detectable binding affinity for phorbol, their mutation would appear not to disrupt the quaternary packing of the C1 domain. In contrast, both of the mutations in the C-terminal loop would affect its interactions with the rest of the protein. The T24L mutation clashes with residue Val^{373} in helix α6 of the DH domain, and the Y26K mutation introduces an unfavorable electrostatic interaction between the lysine and either residue Arg^{402} or residue Lys^{429} in the PH domain. This suggests that the N-terminal loop mutations act to increase the lipophilicity of the C1 domain for membrane binding and the C-terminal loop mutations act to loosen or disrupt the packing of the C1 domain as well as increasing lipophilicity. Both sets of mutations are required for responsiveness to phorbol.

The modeling has a further implication. Because of the proximity of the C-terminal loop of the C1 domain of Vav1 to the α6 helix of the DH domain, a prediction is that an appropriately bulky ligand binding to the C1 domain should disrupt interaction with the DH domain (Fig. 9*B*). Because the C1 domain interaction is required to stabilize the GEF activity of the DH domain, such a ligand might be expected to function as a Vav1 inhibitor.

Comparison of the Binding Affinities of Novel DAG-lactones Designed to Target the Structure of Vav1 C1

The modeling and site-directed mutagenesis results shown above suggested that eliminating the charged Glu residues in the N-terminal loop is necessary (but not sufficient) for restoring phorbol sensitivity to Vav1. We theorized that a ligand bearing a positive charge might similarly "cancel out" the membrane binding penalty imposed on the C1 domain

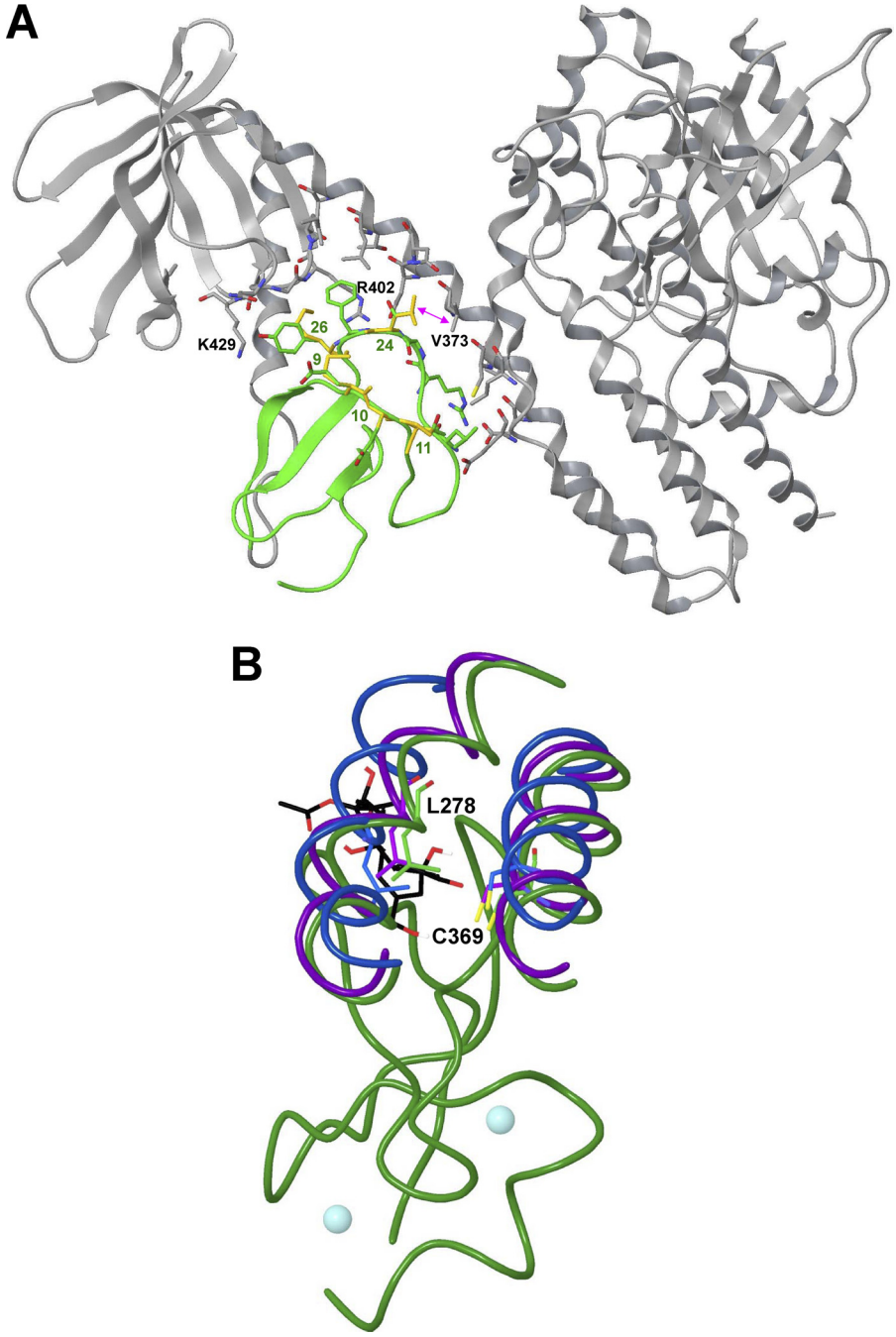

FIGURE 9. *A,* mutations of the C1 domain of Vav1 in the context of adjacent regions (the DH and PH domains) of the full-length protein (15). The C1 domain is colored *green*, and the DH and PH domains are colored *gray*. Mutations in the C1 domain are overlaid with the wild-type residues and colored *yellow*. Residues in the DH and PH domains that conflict with mutations are labeled. A *magenta arrow* marks the steric clash between residue Val^{373} and a Leu at position 24 in the C1 domain. *B,* phorbol 13-acetate docked into the C1 domain of Vav1 (2VRW (15), colored *green*), in the context of its interactions with the DH domain. The other lower resolution crystal structures of Vav1 are aligned as in Fig. 1*B* and colored blue (3KY9) (14) and *purple* (3BJI) (16). Although the orientation of the DH helix differs slightly depending on whether or not the CH domain is present and/or the exchange factor Rac1 is bound (15, 16), in all structures residues in the α3 and α6 helices of the DH domain are positioned to clash with a ligand in the C1 domain binding site. The residues with the strongest steric clashes to phorbol are shown and labeled.

by the negatively charged residues in the N-terminal loop. It is believed that ions in salt-bridged pairs have a reduced desolvation penalty or increased lipophilicity for interaction with the bilayer (61). Such a strategy is used pharmaceutically to improve the intestinal absorption of charged or ionizable drugs (62).

To test this theory we used a series of DAG-lactones. DAG-lactones have proven to provide a high affinity template readily amenable to the introduction of structural variation to probe the nature of ligand-C1 domain interactions (10). The chemical structures of the specific derivatives examined are illustrated in Fig. 10*A*. The various DAG-lactones possess positively charged guanidinium (**6c**) and pyridinium (**8a**–**f**) moieties at the *sn*-2 side chain position. In addition, we included compounds with neutral pyridine (**6a**) and methylindole (**6b**) side chains for comparison.

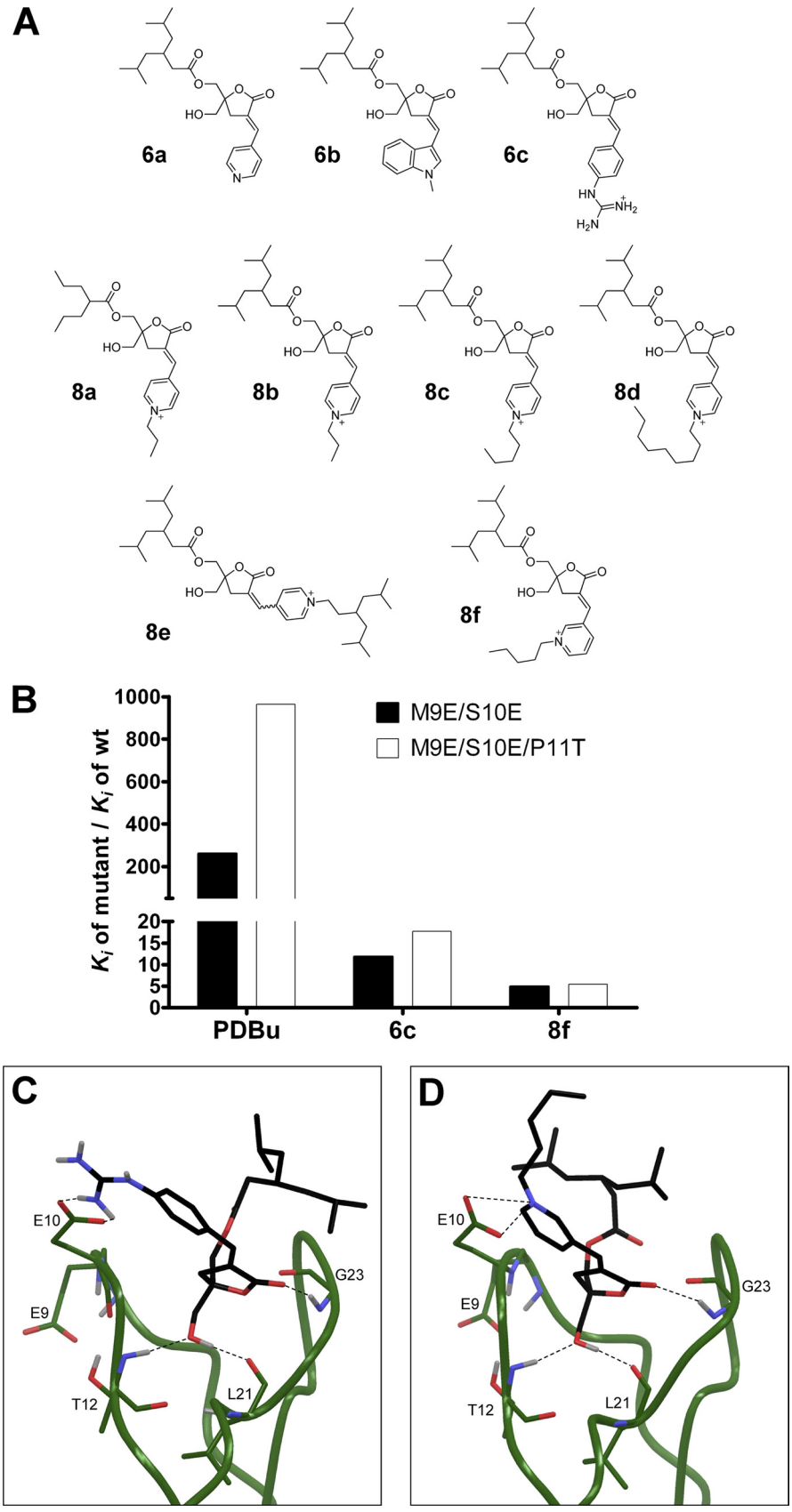

FIGURE 10. *A*, chemical structure of the positively charged diacylglycerol-lactone derivatives. *B*, relative binding affinities for [^{3}H]PDBu and compounds **6c** and **8f** of the double and triple mutants of δC1b. The ratios of the binding affinities of the indicated compounds for the mutant δC1b domain relative to the wild-type δC1b domain are plotted. For [^{3}H]PDBu, the binding affinity was measured as the K_d value; for compounds **6c** and **8f**, it represents the K_i value, as indicated in Table 5. *C* and *D*, charged DAG-lactones **6c** (*C*) and **8f** (*D*) docked into the C1 domain of PKCδ C1b M9E/S10E/P11T. Electrostatic interactions are indicated by *dashed lines*.

TABLE 5

Binding of different DAG-lactone derivatives to δC1b double and triple mutants

The inhibitory dissociation constants (K_i) of δC1 M9E/S10E and of δC1 M9E/S10E/P11T for the DAG lactones were defined in the presence of [^{3}H]PDBu. Values represent the mean ± S.E. ($n = 3$ independent experiments). NA means no activity; ND means not determined.

Compound name	Receptor PKCδ C1b wild type	Receptor PKCδ C1b M9E/S10E	Receptor PKCδ C1b M9E/S10E/P11T
	K_i	K_i	K_i
	nM	nM	nM
[^{3}H]PDBu	0.193 ± 0.005	50.5 ± 2.1	186.1 ± 6.0
6a	10.0 ± 1.5	451 ± 70	ND
6b	0.66 ± 0.6	54.0 ± 4.1	ND
6c	16.1 ± 1.7	191 ± 15	285 ± 28
8a	5810 ± 420	NA	ND
8b	714 ± 97	6690 ± 550	ND
8c	215 ± 19	1760 ± 140	ND
8d	792 ± 67	11680 ± 840	ND
8e	25.2 ± 1.3	1061 ± 27	ND
8f	27.7 ± 6.2	137 ± 15	151 ± 36

To test the relative selectivity of these compounds for the Vav1 C1 structure, we performed *in vitro* competition assays with [^{3}H]PDBu using the double (M9E/S10E) and triple (M9E/S10E/P11T) mutants of δC1b. These mutants retained appreciable binding affinities for [^{3}H]PDBu (which is a prerequisite of our detection of reduced binding in competition assays), however, they displayed marked reduction of binding potency as a result of incorporating Vav1 C1-like residues in their structure. They nevertheless provide useful surrogates as we begin to explore strategies for targeting the specific structural features of Vav1.

As shown in the 1st column of Table 5, introduction of a positive charge into the DAG-lactone yielded compounds that were 83-fold (**6c**) to 30,000-fold (**8a**) weaker in affinity for the wild-type PKCδ C1b domain than was [^{3}H]PDBu. However, when these charged compounds were assayed against the double and triple mutants, the decrease in their binding affinity was significantly less than the decrease in binding affinity seen with neutral PDBu and the neutral DAG-lactones. The binding of [^{3}H]PDBu for the double and triple mutants was reduced 261- and 963-fold, respectively, compared with that for the WT δC1b. The binding affinities of the neutral DAG-lactones **6a** and **6b** to the double mutant were also reduced 45- and 82-fold, respectively, consistent with the loss of binding that we had observed for DOG (Table 2). In contrast, the affinity of the pyridinium-containing lactone **8f** for these mutants decreased only 5-fold in the case of the double mutant (M9E/S10E) and 5.5-fold in the case of the triple mutant (M9E/S10E/P11T). Similarly, the affinity of the guanidinium-containing lactone **6c** decreased only 12- and 17-fold, respectively. The relative binding affinities of these two charged compounds and [^{3}H]PDBu to the double and triple mutants *versus* the wild-type δC1b domain are depicted in Fig. 10*B*.

Within the pyridinium-containing DAG-lactones, the greater affinity of **8f** for the double mutant, relative to its less active isomer **8c**, suggests that the exact orientation of the positive charge in the pyridinium ring is important for effective neutralization. Comparing compound **8c**, with a 5-carbon chain on the pyridinium ring, to the less potent compounds **8b** (3-carbon chain) and **8d** (9-carbon chain) suggests that the exact length of this alkyl chain is also important. The presence and extent of branching in the alkyl groups on either the *sn*-1 or the *sn*-2 side chains also affect their binding affinities. We have shown previously that subtle differences in the chemical structure of the side chains on the DAG-lactone template can produce widely varying biological responses (63), due in part to differences in the degree of penetration of charged DAG-lactones into the membrane (40). These results suggest that the 3-pyridyl and guanidyl series of compounds could be explored further to optimize their alkyl substituents and examine their biological effects against charged C1 domains *in vivo*.

To rationalize and visualize our results, we docked the highest affinity charged DAG-lactones **6c** and **8f** into the triple (M9E/S10E/P11T) mutant structure of δC1b. Because docking holds the receptor structure fixed, we followed it with a conformational search of the ligand and the charged binding site side chains to allow them to form favorable interactions. As shown in Fig. 10, *C* and *D*, Glu^{10} can easily form a salt bridge to both the charged nitrogen in the pyridinium group of DAG-lactone **8f** and the guanidinium group of DAG-lactone **6c**. The additional alkyl chain on the *sn*-2 pyridinium ring of compound **8f** provides greater hydrophobic coverage over the top surface of the C1 domain, which could promote the insertion of this complex into the bilayer, and explain its slightly better affinity.

These results illustrate that the DAG-lactone template is in principle structurally capable of forming ion-pair interactions with charged residues in the C1 domain binding site. Although these compounds represent only an early stage in the design of agents targeting the C1 domain of Vav1, they support the concept that appropriate interaction with the unique negatively charged residues at positions 9 and 10 may represent one element in the strategy.

DISCUSSION

C1 domain-containing proteins have been classified into two major groups based on ligand responsiveness (11). Typical C1 domains bind DAG/phorbol esters, whereas atypical C1 domains do not. Previous findings of our laboratory with the atypical PKCs (aPKCs) indicated that the family of atypical C1 domains could be further divided (13). c-Raf and KSR exemplify atypical C1 domains with a structurally distorted binding pocket that is not compatible with ligand interactions, whereas the aPKCs have a C1 domain that retains a compatible binding cleft geometry but possesses other characteristics that interfere with efficient ligand interactions, namely the four arginine residues lining the rim of the binding pocket can fold into the cleft, effectively competing with ligand. Vav1 is another member of the subclass of atypical C1 domains with compatible binding pocket geometry and the potential to interact with DAG analogs. In this study, we showed that the basis for the lack of activity of Vav1 appears to be different from that in the case of the aPKCs. Modeling emphasizes that the rim of the binding cleft of Vav1 displays enhanced hydrophilicity, interfering with membrane insertion and stabilization of the ternary binding complex. We identified four hydrophilic residues in Vav1 C1 (Glu^9, Glu^{10}, Thr^{11}, and Thr^{24}) that drive its lack of binding. Beyond the hydrophobic cap, C1 domains have an annulus of charged residues that interact with negatively charged phospholipid headgroups. In Vav1, we identified an additional resi-

due (Tyr^{26}) in this annular region that further contributes to the inhibition of binding.

A striking finding, for Vav1, as well as for the aPKCs, was that in neither case did a critical residue cause a major structural change in the binding pocket that abrogated ligand affinity. Rather, lack of binding represented the cumulative effect of the otherwise modest impact of multiple individual residues on binding potency, a mechanism of "death by a thousand cuts."

Our experimental approaches using forward and back mutagenesis afforded somewhat different conclusions about the importance of different residues. The δC1b single site mutants indicated an almost uniform contribution for each of the five unique residues to the lack of ligand binding. However, the findings with the Vav1 C1 quadruple mutants (analogous to δC1b mutants in this setting) suggested a more robust effect for each residue in the lack of ligand binding, and in addition they revealed a more prominent impact for the Glu^9 and Pro^{11} residues on binding potency. These differences, together with the lack of additivity of the effects upon multiple changes in residues, provide a reminder that the context, *i.e.* the influence of the other residues in the C1 domain, on the overall behavior cannot be ignored. It also is consistent with our calculations that the overall lipophilicity of the δC1b is greater than that of the Vav1 C1 domain, even after introduction of the mutated residues.

Because of the structural similarities between the C1 domains of Vav1, Vav2, and Vav3, we speculate that factors similar to those that interfere with the phorbol ester binding of Vav1 might also apply in the cases of Vav2 and Vav3. Likewise, Vav orthologs have been described in both *Caenorhabditis elegans* and in *Drosophila melanogaster* (64, 65). Evaluation of their behavior should further extend our understanding of C1 domain structure-function relationships. A number of other C1 domains reported either to be weakly sensitive or not sensitive to phorbol esters or diacylglycerol, such as those of RasGRP2 (66) or PKCθ C1a (67, 68), afford a further opportunity to probe factors influencing C1 domain ligand interactions. As with Vav1, such structural differences in turn may afford the opportunity for the design of specific ligands exploiting these structural differences.

Vav1 represents a therapeutic target rich in potential applications. Vav1 is an essential regulator of leukocyte functions, including T-cell activation and development, B-cell function, induction of the killing function of Natural Killer cells, and the migration and phagocytic activity of macrophages (22). Although mutated versions of Vav1 have never been described in human cancer, the aberrant expression of the wild-type Vav1 in several malignancies (*e.g.* melanoblastoma, pancreatic ductal adenocarcinoma) suggests that it can play a pivotal role in tumorigenesis and tumor progression (28, 29). Finally, the actin cytoskeleton remodeling mediated by Vav1 through the Rho/Rac1 family of small GTPases may contribute to the increased invasive and metastatic potential of neoplastic cells (69).

The C1 domain has been shown to play a critical role in the enzymatic function of Vav1 (34). Our current understanding, from the x-ray crystallographic analysis of Rapley *et al.* (15), is that there is a complex network of intramolecular contacts between the C1 (and the PH) domain and the DH domain, which help to restrict the flexibility of a crucial α6 helix in the DH domain, thereby stabilizing it in a conformation that facilitates maximal exchange activity. The solvent-exposed cavity formed from the apparent binding pocket of the C1 domain lies in the vicinity of these intimate interactions. In fact, the authors identified that Arg^{22}, Thr^{24}, and Phe^{25} (using the C1 domain terminology) form very significant connections with the residues situated at the α6-helix of DH domain within this DH-C1 interface. These residues are located at the C-terminal loop of the binding pocket of C1. Our findings reveal that the Vav1 C1 domain indeed possesses the potential to accommodate DAG/phorbol esters. Although the presence of unique residues along the binding cleft renders the molecule noncompatible with membrane insertion, these residues provide a unique opportunity for drug design, engineering specific contacts. Given the high selectivity of phorbol esters, DAG-lactones, and related compounds for C1 domains (10), the combination of this chemistry with further features exploiting the specific features of a class of atypical C1 domain targets such as those of Vav should provide great specificity. Our current understanding makes the strong prediction that such ligand binding, by disrupting the C1 domain-DH domain interactions, should inhibit the exchange activity of Vav.

Although these possibilities remain speculative, in this study we tested a series of diacylglycerol-lactones to begin to explore this concept. A strategy adopted by the Marquez and Blumberg group (10) for efficient synthesis of ligands that interact with the binding pockets of the C1 domain-containing proteins (most notably PKCs) was the cyclization of the structure of the low affinity endogenous ligand DAG to generate the conformationally constrained DAG-lactones, which with optimization can achieve affinities approaching high pM. Using this approach, we have previously developed the novel DAG-lactone 130C037, which displayed marked selectivity among the recombinant C1a and C1b domains of PKCα and PKCδ, as well as substantial selectivity for the guanyl exchange factor RasGRP relative to PKCα (49). We have further shown the potential of combinatorial chemistry for identification of diacylglycerol-lactones with selectivity for any of a variety of biological end points (63). Although the diacylglycerol-lactones described here were only of moderate nanomolar affinity, several showed markedly enhanced selectivity, compared with the prototypical ligand PDBu, for the δC1b domain containing several of the Vav1-specific residues, which we used as a surrogate for the wild-type Vav1 C1 structure. These DAG-lactone derivatives contained a positively charged side chain that had the potential to interact with the negatively charged glutamic acid residues. Although such compounds provide proof of principle, it should be emphasized that they represent only a first step.

REFERENCES

1. Carrasco, S., and Mérida, I. (2007) Diacylglycerol, when simplicity becomes complex. *Trends Biochem. Sci.* **32,** 27–36
2. Newton, A. C. (1995) Protein kinase C. Structure, function, and regulation. *J. Biol. Chem.* **270,** 28495–28498
3. Kazanietz, M. G. (2002) Novel "nonkinase" phorbol ester receptors. The C1 domain connection. *Mol. Pharmacol.* **61,** 759–767
4. Blumberg, P. M., Kedei, N., Lewin, N. E., Yang, D., Czifra, G., Pu, Y., Peach, M. L., and Marquez, V. E. (2008) Wealth of opportunity. The C1 domain as

a target for drug development. *Curr. Drug Targets* **9,** 641–652
5. Griner, E. M., and Kazanietz, M. G. (2007) Protein kinase C and other diacylglycerol effectors in cancer. *Nat. Rev. Cancer* **7,** 281–294
6. Xu, R. X., Pawelczyk, T., Xia, T. H., and Brown, S. C. (1997) NMR structure of a protein kinase C-γ phorbol-binding domain and study of protein-lipid micelle interactions. *Biochemistry* **36,** 10709–10717
7. Zhang, G., Kazanietz, M. G., Blumberg, P. M., and Hurley, J. H. (1995) Crystal structure of the Cys-2 activator-binding domain of protein kinase Cδ in complex with phorbol ester. *Cell* **81,** 917–924
8. Stewart, M. D., Morgan, B., Massi, F., and Igumenova, T. I. (2011) Probing the determinants of diacylglycerol binding affinity in the C1B domain of protein kinase Cα. *J. Mol. Biol.* **408,** 949–970
9. Pak, Y., Enyedy, I. J., Varady, J., Kung, J. W., Lorenzo, P. S., Blumberg, P. M., and Wang, S. (2001) Structural basis of binding of high affinity ligands to protein kinase C. Prediction of the binding modes through a new molecular dynamics method and evaluation by site-directed mutagenesis. *J. Med. Chem.* **44,** 1690–1701
10. Marquez, V. E., and Blumberg, P. M. (2003) Synthetic diacylglycerols (DAG) and DAG-lactones as activators of protein kinase C (PK-C). *Acc. Chem. Res.* **36,** 434–443
11. Hurley, J. H., Newton, A. C., Parker, P. J., Blumberg, P. M., and Nishizuka, Y. (1997) Taxonomy and function of C1 protein kinase C homology domains. *Protein Sci.* **6,** 477–480
12. Colón-González, F., and Kazanietz, M. G. (2006) C1 domains exposed. From diacylglycerol binding to protein-protein interactions. *Biochim. Biophys. Acta* **1761,** 827–837
13. Pu, Y., Peach, M. L., Garfield, S. H., Wincovitch, S., Marquez, V. E., and Blumberg, P. M. (2006) Effects on ligand interaction and membrane translocation of the positively charged arginine residues situated along the C1 domain binding cleft in the atypical protein kinase C isoforms. *J. Biol. Chem.* **281,** 33773–33788
14. Yu, B., Martins, I. R., Li, P., Amarasinghe, G. K., Umetani, J., Fernandez-Zapico, M. E., Billadeau, D. D., Machius, M., Tomchick, D. R., and Rosen, M. K. (2010) Structural and energetic mechanisms of cooperative autoinhibition and activation of Vav1. *Cell* **140,** 246–256
15. Rapley, J., Tybulewicz, V. L., and Rittinger, K. (2008) Crucial structural role for the PH and C1 domains of the Vav1 exchange factor. *EMBO Rep.* **9,** 655–661
16. Chrencik, J. E., Brooun, A., Zhang, H., Mathews, I. I., Hura, G. L., Foster, S. A., Perry, J. J., Streiff, M., Ramage, P., Widmer, H., Bokoch, G. M., Tainer, J. A., Weckbecker, G., and Kuhn, P. (2008) Structural basis of guanine nucleotide exchange mediated by the T-cell essential Vav1. *J. Mol. Biol.* **380,** 828–843
17. Gulbins, E., Coggeshall, K. M., Baier, G., Telford, D., Langlet, C., Baier-Bitterlich, G., Bonnefoy-Berard, N., Burn, P., Wittinghofer, A., and Altman, A. (1994) Direct stimulation of Vav guanine nucleotide exchange activity for Ras by phorbol esters and diglycerides. *Mol. Cell. Biol.* **14,** 4749–4758
18. Kazanietz, M. G., Bustelo, X. R., Barbacid, M., Kolch, W., Mischak, H., Wong, G., Pettit, G. R., Bruns, J. D., and Blumberg, P. M. (1994) Zinc finger domains and phorbol ester pharmacophore. Analysis of binding to mutated form of protein kinase Cζ and the *vav* and c-*raf* proto-oncogene products. *J. Biol. Chem.* **269,** 11590–11594
19. Bustelo, X. R. (2000) Regulatory and signaling properties of the Vav family. *Mol. Cell. Biol.* **20,** 1461–1477
20. Hornstein, I., Mortin, M. A., and Katzav, S. (2003) DroVav, the *Drosophila melanogaster* homologue of the mammalian Vav proteins, serves as a signal transducer protein in the Rac and DER pathways. *Oncogene* **22,** 6774–6784
21. Tybulewicz, V. L. (2005) Vav family proteins in T-cell signaling. *Curr. Opin. Immunol.* **17,** 267–274
22. Bustelo, X. R. (2001) Vav proteins, adaptors and cell signaling. *Oncogene* **20,** 6372–6381
23. Katzav, S., Martin-Zanca, D., and Barbacid, M. (1989) *vav*, a novel human oncogene derived from a locus ubiquitously expressed in hematopoietic cells. *EMBO J.* **8,** 2283–2290
24. Movilla, N., and Bustelo, X. R. (1999) Biological and regulatory properties of Vav-3, a new member of the Vav family of oncoproteins. *Mol. Cell. Biol.* **19,** 7870–7885
25. Henske, E. P., Short, M. P., Jozwiak, S., Bovey, C. M., Ramlakhan, S., Haines, J. L., and Kwiatkowski, D. J. (1995) Identification of VAV2 on 9q34 and its exclusion as the tuberous sclerosis gene *TSC1*. *Ann. Hum. Genet.* **59,** 25–37
26. Dustin, M. L., and Shaw, A. S. (1999) Costimulation. Building an immunological synapse. *Science* **283,** 649–650
27. Fischer, K. D., Zmuldzinas, A., Gardner, S., Barbacid, M., Bernstein, A., and Guidos, C. (1995) Defective T-cell receptor signaling and positive selection of Vav-deficient $CD4^+$ $CD8^+$ thymocytes. *Nature* **374,** 474–477
28. Katzav, S. (2009) Vav1. A hematopoietic signal transduction molecule involved in human malignancies. *Int. J. Biochem. Cell Biol.* **41,** 1245–1248
29. Katzav, S. (2007) Flesh and blood. The story of *Vav1*, a gene that signals in hematopoietic cells but can be transforming in human malignancies. *Cancer Lett.* **255,** 241–254
30. Fernandez-Zapico, M. E., Gonzalez-Paz, N. C., Weiss, E., Savoy, D. N., Molina, J. R., Fonseca, R., Smyrk, T. C., Chari, S. T., Urrutia, R., and Billadeau, D. D. (2005) Ectopic expression of VAV1 reveals an unexpected role in pancreatic cancer tumorigenesis. *Cancer Cell* **7,** 39–49
31. Prieto-Sánchez, R. M., Hernández, J. A., García, J. L., Gutiérrez, N. C., San Miguel, J., Bustelo, X. R., and Hernández, J. M. (2006) Overexpression of the VAV proto-oncogene product is associated with B-cell chronic lymphocytic leukemia displaying loss on 13q. *Br. J. Haematol.* **133,** 642–645
32. Bartolomé, R. A., Molina-Ortiz, I., Samaniego, R., Sánchez-Mateos, P., Bustelo, X. R., and Teixidó, J. (2006) Activation of Vav/Rho GTPase signaling by CXCL12 controls membrane-type matrix metalloproteinase-dependent melanoma cell invasion. *Cancer Res.* **66,** 248–258
33. Movilla, N., Dosil, M., Zheng, Y., and Bustelo, X. R. (2001) How Vav proteins discriminate the GTPases Rac1 and RhoA from Cdc42. *Oncogene* **20,** 8057–8065
34. Booden, M. A., Campbell, S. L., and Der, C. J. (2002) Critical but distinct roles for the pleckstrin homology and cysteine-rich domains as positive modulators of Vav2 signaling and transformation. *Mol. Cell. Biol.* **22,** 2487–2497
35. Zugaza, J. L., López-Lago, M. A., Caloca, M. J., Dosil, M., Movilla, N., and Bustelo, X. R. (2002) Structural determinants for the biological activity of Vav proteins. *J. Biol. Chem.* **277,** 45377–45392
36. Heo, J., Thapar, R., and Campbell, S. L. (2005) Recognition and activation of Rho GTPases by Vav1 and Vav2 guanine nucleotide exchange factors. *Biochemistry* **44,** 6573–6585
37. Lewin, N. E., and Blumberg, P. M. (2003) [^{3}H]Phorbol 12,13-dibutyrate binding assay for protein kinase C and related proteins. *Methods Mol. Biol.* **233,** 129–156
38. Wang, Q. J., Fang, T. W., Nacro, K., Marquez, V. E., Wang, S., and Blumberg, P. M. (2001) Role of hydrophobic residues in the C1b domain of protein kinase Cδ on ligand and phospholipid interactions. *J. Biol. Chem.* **276,** 19580–19587
39. El Kazzouli, S., Lewin, N. E., Blumberg, P. M., and Marquez, V. E. (2008) Conformationally constrained analogues of diacylglycerol. 30. An investigation of diacylglycerol-lactones containing heteroaryl groups reveals compounds with high selectivity for Ras guanyl nucleotide-releasing proteins. *J. Med. Chem.* **51,** 5371–5386
40. Raifman, O., Kolusheva, S., El Kazzouli, S., Sigano, D. M., Kedei, N., Lewin, N. E., Lopez-Nicolas, R., Ortiz-Espin, A., Gomez-Fernandez, J. C., Blumberg, P. M., Marquez, V. E., Corbalan-Garcia, S., and Jelinek, R. (2010) Membrane-surface anchoring of charged diacylglycerol-lactones correlates with biological activities. *ChemBioChem* **11,** 2003–2009
41. Jones, G., Willett, P., Glen, R. C., Leach, A. R., and Taylor, R. (1997) Development and validation of a genetic algorithm for flexible docking. *J. Mol. Biol.* **267,** 727–748
42. MacroModel, Version 9.8, Schrödinger, LLC, New York 2010
43. Steinkellner, G., Rader, R., Thallinger, G. G., Kratky, C., and Gruber, K. (2009) VASCo. Computation and visualization of annotated protein surface contacts. *BMC Bioinformatics* **10,** 32
44. Ghose, A. K., Viswanadhan, V. N., and Wendoloski, J. J. (1998) Prediction of hydrophobic (lipophilic) properties of small organic molecules using fragmental methods. An analysis of ALOGP and CLOGP methods. *J. Phys.*

Chem. A **102,** 3762–3772
45. Sanner, M. F., Olson, A. J., and Spehner, J. C. (1996) Reduced surface. An efficient way to compute molecular surfaces. *Biopolymers* **38,** 305–320
46. Heiden, W., Moeckel, G., and Brickmann, J. (1993) A new approach to analysis and display of local lipophilicity/hydrophilicity mapped on molecular surfaces. *J. Comput. Aided Mol. Des.* **7,** 503–514
47. Canagarajah, B., Leskow, F. C., Ho, J. Y., Mischak, H., Saidi, L. F., Kazanietz, M. G., and Hurley, J. H. (2004) Structural mechanism for lipid activation of the Rac-specific GAP, β2-chimerin. *Cell* **119,** 407–418
48. Leonard, T. A., Róycki, B., Saidi, L. F., Hummer, G., and Hurley, J. H. (2011) Crystal structure and allosteric activation of protein kinase C βII. *Cell* **144,** 55–66
49. Pu, Y., Perry, N. A., Yang, D., Lewin, N. E., Kedei, N., Braun, D. C., Choi, S. H., Blumberg, P. M., Garfield, S. H., Stone, J. C., Duan, D., and Marquez, V. E. (2005) A novel diacylglycerol-lactone shows marked selectivity *in vitro* among C1 domains of protein kinase C (PKC) isoforms α and δ as well as selectivity for RasGRP compared with PKCα. *J. Biol. Chem.* **280,** 27329–27338
50. Stahelin, R. V., Digman, M. A., Medkova, M., Ananthanarayanan, B., Rafter, J. D., Melowic, H. R., and Cho, W. (2004) Mechanism of diacylglycerol-induced membrane targeting and activation of protein kinase Cδ. *J. Biol. Chem.* **279,** 29501–29512
51. Irie, K., Nakagawa, Y., and Ohigashi, H. (2004) Indolactam and benzolactam compounds as new medicinal leads with binding selectivity for C1 domains of protein kinase C isozymes. *Curr. Pharm. Des.* **10,** 1371–1385
52. Oancea, E., Teruel, M. N., Quest, A. F., and Meyer, T. (1998) Green fluorescent protein (GFP)-tagged cysteine-rich domains from protein kinase C as fluorescent indicators for diacylglycerol signaling in living cells. *J. Cell Biol.* **140,** 485–498
53. Farah, C. A., Nagakura, I., Weatherill, D., Fan, X., and Sossin, W. S. (2008) Physiological role for phosphatidic acid in the translocation of the novel protein kinase C Apl II in *Aplysia* neurons. *Mol. Cell. Biol.* **28,** 4719–4733
54. Cho, W., and Stahelin, R. V. (2005) Membrane-protein interactions in cell signaling and membrane trafficking. *Annu. Rev. Biophys. Biomol. Struct.* **34,** 119–151
55. Ahmed, S., Kozma, R., Lee, J., Monfries, C., Harden, N., and Lim, L. (1991) The cysteine-rich domain of human proteins, neuronal chimaerin, protein kinase C, and diacylglycerol kinase binds zinc. Evidence for the involvement of a zinc-dependent structure in phorbol ester binding. *Biochem. J.* **280,** 233–241
56. Kazanietz, M. G., Wang, S., Milne, G. W., Lewin, N. E., Liu, H. L., and Blumberg, P. M. (1995) Residues in the second cysteine-rich region of protein kinase Cδ relevant to phorbol ester binding as revealed by site-directed mutagenesis. *J. Biol. Chem.* **270,** 21852–21859
57. Dries, D. R., Gallegos, L. L., and Newton, A. C. (2007) A single residue in the C1 domain sensitizes novel protein kinase C isoforms to cellular diacylglycerol production. *J. Biol. Chem.* **282,** 826–830
58. Chen, J., Deng, F., Li, J., and Wang, Q. J. (2008) Selective binding of phorbol esters and diacylglycerol by individual C1 domains of the PKD family. *Biochem. J.* **411,** 333–342
59. Furet, P., Sele, A., and Cohen, N. C. (1988) 3D molecular lipophilicity potential profiles. A new tool in molecular modeling. *J. Mol. Graphics* **6,** 182–189
60. Delano, W. L. (2002) *The PyMOL Molecular Graphics System,* Version 0.99 Ed., DeLano Scientific, Palo Alto, CA
61. Neubert, R. (1989) Ion pair transport across membranes. *Pharm. Res.* **6,** 743–747
62. Miller, J. M., Dahan, A., Gupta, D., Varghese, S., and Amidon, G. L. (2010) Enabling the intestinal absorption of highly polar antiviral agents. Ion-pair facilitated membrane permeation of zanamivir heptyl ester and guanidino oseltamivir. *Mol. Pharm.* **7,** 1223–1234
63. Duan, D., Sigano, D. M., Kelley, J. A., Lai, C. C., Lewin, N. E., Kedei, N., Peach, M. L., Lee, J., Abeyweera, T. P., Rotenberg, S. A., Kim, H., Kim, Y. H., El Kazzouli, S., Chung, J. U., Young, H. A., Young, M. R., Baker, A., Colburn, N. H., Haimovitz-Friedman, A., Truman, J. P., Parrish, D. A., Deschamps, J. R., Perry, N. A., Surawski, R. J., Blumberg, P. M., and Marquez, V. E. (2008) Conformationally constrained analogues of diacylglycerol. 29. Cells sort diacylglycerol-lactone chemical zip codes to produce diverse and selective biological activities. *J. Med. Chem.* **51,** 5198–5220
64. Norman, K. R., Fazzio, R. T., Mellem, J. E., Espelt, M. V., Strange, K., Beckerle, M. C., and Maricq, A. V. (2005) The Rho/Rac-family guanine nucleotide exchange factor VAV-1 regulates rhythmic behaviors in *C. elegans*. *Cell* **123,** 119–132
65. Dekel, I., Russek, N., Jones, T., Mortin, M. A., and Katzav, S. (2000) Identification of the *Drosophila melanogaster* homologue of the mammalian signal transducer protein, Vav. *FEBS Lett.* **472,** 99–104
66. Johnson, J. E., Goulding, R. E., Ding, Z., Partovi, A., Anthony, K. V., Beaulieu, N., Tazmini, G., Cornell, R. B., and Kay, R. J. (2007) Differential membrane binding and diacylglycerol recognition by C1 domains of RasGRPs. *Biochem. J.* **406,** 223–236
67. Irie, K., Nakagawa, Y., and Ohigashi, H. (2005) Toward the development of new medicinal leads with selectivity for protein kinase C isozymes. *Chem. Rec.* **5,** 185–195
68. Melowic, H. R., Stahelin, R. V., Blatner, N. R., Tian, W., Hayashi, K., Altman, A., and Cho, W. (2007) Mechanism of diacylglycerol-induced membrane targeting and activation of protein kinase Cθ. *J. Biol. Chem.* **282,** 21467–21476
69. Hornstein, I., Alcover, A., and Katzav, S. (2004) Vav proteins, masters of the world of cytoskeleton organization. *Cell. Signal.* **16,** 1–11